

Early-type galaxy speciation: Elliptical (E) and ellicular (ES) galaxies in the $M_{\text{bh}}-M_{\star,\text{sph}}$ diagram, and a merger-driven explanation for the origin of ES galaxies, anti-truncated stellar discs in lenticular (S0) galaxies, and the Sérsicification of E galaxy light profiles

Alister W. Graham¹★

¹ Centre for Astrophysics and Supercomputing, Swinburne University of Technology, Hawthorn, VIC 3122, Australia

Accepted XXX. Received YYY; in original form ZZZ

ABSTRACT

In a recent series of papers, supermassive black holes were used to discern pathways in galaxy evolution. By considering the black holes’ coupling with their host galaxy’s bulge/spheroid, the progression of mass within each component has shed light on the chronological sequence of galaxy speciation. Offsets between the galaxy-morphology-dependent $M_{\text{bh}}-M_{\star,\text{sph}}$ scaling relations trace a pattern of ‘punctuated equilibrium’ arising from merger-driven transitions between galaxy types, such as from spirals to dust-rich lenticulars and further to ‘ellicular’ and elliptical galaxies. This study delves deeper into the distinction between the ellicular galaxies — characterised by their intermediate-scale discs — and elliptical galaxies. Along the way, it is shown how some anti-truncated large-scale discs in lenticular galaxies can arise from the coexistence of a steep intermediate-scale disc and a relatively shallow large-scale disc. This observation undermines application of the popular exponential-disc plus Sérsic-bulge model for lenticular galaxies and suggests some past bulge mass measurements have been overestimated. Furthermore, it is discussed how merger-driven disc-heating and blending likely leads to the spheroidalisation of discs and the conglomeration of multiple discs leads to the (high- n) Sérsicification of light profiles. The ellicular and elliptical galaxy distribution in the $M_{\text{bh}}-M_{\star,\text{sph}}$ diagram is explored relative to major-merger-built lenticular galaxies and brightest cluster galaxies. The (super-)quadratic $M_{\text{bh}}-M_{\star}$ relations, presented herein, for merger-built systems should aid studies of massive black hole collisions and the gravitational wave background. Finally, connections to dwarf compact elliptical and ultra-compact dwarf galaxies, with their 100-1000 times higher $M_{\text{bh}}/M_{\star,\text{sph}}$ ratios, are presented.

Key words: galaxies: bulges – galaxies: elliptical and lenticular, cD – galaxies: structure – galaxies: interactions – galaxies: evolution – (galaxies:) quasars: supermassive black holes

1 INTRODUCTION

Over the past decade, the (black hole mass, M_{bh})-(spheroid stellar mass, $M_{\star,\text{sph}}$) diagram (Kormendy & Richstone 1995; Magorian et al. 1998; Wandell 1999; Laor 2001) has steadily revealed clues about the coevolution of galaxies and their central black hole. For example, the dust-poor, low-mass lenticular (S0) galaxies appear to be primarily faded primaevial S0 galaxies that need never have sported a spiral pattern. They define a quasi-quadratic $M_{\text{bh}}-M_{\star,\text{sph}}$ relation with a slope of 2.39 ± 0.81 and have $M_{\text{bh}}/M_{\star,\text{sph}}$ ratios that are, on average, five times higher than in spiral (S) galaxies with the same $M_{\star,\text{sph}}$ (Graham 2023c). This disfavors these S0 galaxies being faded S galaxies that lost their gas and spiral pattern. This population of S0 galaxies has also been highlighted for

having an order of magnitude higher M_{bh} -to-(galaxy stellar mass, $M_{\star,\text{gal}}$) ratio than the S galaxies and merger-built early-type galaxies (ETGs) that collectively defined the Jeans-Reynolds-Hubble sequence (Jeans 1919; Reynolds 1925; Hubble 1926).¹

to be more closely connected with their morphology than their $M_{\text{bh}}/M_{\star,\text{sph}}$ ratio, alleged to dictate active galactic nuclei (AGN) feedback, itself widely reported to regulate star formation. Whereas bipolar jets from a central black hole may not directly impact the

¹ Sir James Jeans embraced and advocated for the spheroid-to-spiral evolutionary sequence developed in the ‘nebular hypothesis’ (Swedenborg 1734; Kant 1755; Laplace 1796). Reynolds introduced the notion of a bridging population of S0 galaxies, which Hubble (1936) adopted when he updated his schema, which had initially introduced the ‘early’ and ‘late’ galaxy terminology to reflect the centuries-old evolutionary scheme (see Graham 2019).

★ E-mail: AGraham@swin.edu.au

bulk of a galaxy disc’s interstellar medium (ISM) — although radio-mode feedback can maintain an X-ray hot halo that curtails disc star formation (Benson et al. 2003) — mergers can have a galaxy-wide influence on star formation and build bulges through the redistribution of disc stars, thereby setting the galaxy morphology. Therefore, galaxy morphology, which reflects a galaxy’s accretion/merger history, should probably receive more attention than it has regarding galaxy-black hole coevolution.²

To continue, major gas-rich, aka ‘wet’, S galaxy mergers can transform S galaxies into high-mass, dust-rich S0 galaxies (e.g. NGC 5128, NGC 4753) that have been observed to define their own $M_{\text{bh}}-M_{\star,\text{sph}}$ relation separate from the low-mass dust-poor S0 galaxies and separate from the S galaxies. These high-mass S0 galaxies can have more massive bulges than observed in S galaxies (Burstein et al. 2005; Graham 2023b), again disfavouring a faded S galaxy origin for much of this population. Kaviraj et al. (2012), see also Yoon & Lim (2020), report that two-thirds of nearby ETGs with prominent dust lanes are morphologically disturbed, suggestive of a merger origin, and they are accompanied by bluer $NUV-r$ colours. This population has low-to-intermediate levels of star formation midway between that of elliptical (E) and S galaxies (Graham et al. 2024). An additional round of merging of these massive galaxies will likely produce E galaxies that leave the ‘green valley’ or ‘green mountain’ (Eales et al. 2018; Graham et al. 2024). The offset nature of the E galaxies from the merger-built S0 galaxies in the $M_{\text{bh}}-M_{\star,\text{sph}}$ (and $M_{\text{bh}}-\sigma$; Ferrarese & Merritt 2000) diagram confirms a picture of relatively gas-poor, aka ‘dry’ merging (Graham & Sahu 2023a; Graham 2023a), as do their depleted stellar cores (Begelman et al. 1980; Faber et al. 1997; Graham 2004; Gualandris & Merritt 2012). Once these E galaxies reside in a hot X-ray gas halo (either of their own making due to, say, collision-induced shock-heating, stellar winds and supernova explosions, or from their group or cluster environment), and with the shelter of a disc now gone, their dust and cold gas tend not to survive (Draine & Salpeter 1979; Benson et al. 2003; Galliano et al. 2021).

The above cascade of mergers (e.g. Guo et al. 2011) erases the ordered motion of stars in discs and builds up a galaxy’s spheroidal component (e.g. Quinn et al. 1993) and black hole (e.g. Merritt et al. 2007; Kulkarni & Loeb 2012). The ensuing galaxy sequence described in Graham (2023c) (i) reverses the original direction of assumed evolution in the Jeans-Reynolds-Hubble sequence, (ii) adds a new population of primaevial S0 galaxies, and (iii) includes both an accretion- and merger-driven pathway for these S0 galaxies that is also evident in the colour-magnitude diagram (Graham 2024). The galaxy family tree can be thought of as an increasing entropy sequence (Richstone & Tremaine 1988; Lima Neto et al. 1999) in which ordered rotation becomes disordered. Rather than following a near-linear $M_{\text{bh}}-M_{\star,\text{sph}}$ relation, the major-merger-built galaxies roughly follow an $M_{\text{bh}}-M_{\star,\text{sph}}^2$ (or steeper) relation with (galaxy type)-dependent zero-points. This has relevance beyond understanding and quantifying the coevolution of galaxies and black holes, extending to, for example, gravitational wave surveys (e.g. Rosado et al. 2015; Amaro-Seoane et al. 2023; Agazie et al. 2024;

² There is benefit in separating the S0 galaxies from the E galaxies, and further separating dust-poor primordial S0 galaxies from S0 galaxies built via major-wet-mergers. Indeed, exploration of galaxy morphology relations with other properties may be befuddled unless the S0s are separated according to their place in the galaxy speciation chain. For example, this is why S galaxies initially appeared as a bridging population between E and (all, combined) S0 galaxies in the $(M_{\text{bh}}/M_{\star,\text{sph}})-M_{\star,\text{sph}}$ diagram (Sahu et al. 2019a).

Torres-Orjuela et al. 2023). Furthermore, additional refined details are already getting teased out of the $M_{\text{bh}}-M_{\star,\text{sph}}$ diagram, such as the offset nature of brightest cluster galaxies (BCGs) from regular (non-BCG) E galaxies, revealing the BCGs have been, on average, built from a major dry merger of two non-BCG E galaxies (or some equivalent combination of mass, e.g. 1 E + 2 S0 galaxies). Moreover, with dry mergers establishing the E and BCG galaxy-black hole scaling relations (Graham & Sahu 2023a), AGN feedback has been relegated in these systems to simply a maintenance role.

Prior to the formation of pressure-supported (aka dynamically-hot) discless E galaxies, one encounters the ellicular (ES) galaxies (Liller 1966) with intermediate-scale discs that do not dominate the light at large radii. ES galaxies are not quite the same as ‘disc ellipticals’ (Nieto et al. 1988, aka ‘discy ellipticals’), which refers to alleged E galaxies with pointed isophotes indicative of a somewhat or fully edge-on disc. The latter designation can include S0 galaxies with a large-scale disc and exclude ES galaxies with a somewhat face-on and, thus, overlooked disc. As presented in Graham (2023c), the ES,e subtype is more akin to E galaxies, while the ES,b subtype encompasses compact massive galaxies such as NGC 1277 (Trujillo et al. 2014; Graham et al. 2016a) that appear more like the bulges of high-mass S0 galaxies, themselves resembling ‘red nuggets’ at $z \approx 2.5 \pm 1$ (Daddi et al. 2005; Damjanov et al. 2009; Graham et al. 2015; Hon et al. 2022, 2023). While it is known that E4-E7 galaxies are (overwhelmingly) S0 galaxies with (often missed) large-scale discs (Liller 1966; Gorbachev 1970; Michard 1984; Capaccioli et al. 1990; van den Bergh 1990), there are still hidden discs in galaxies that are routinely designated E0-E3 or S0. Emsellem et al. (2011) recognised some of these galaxies (e.g. NGC 4476, NGC 4528, NGC 5631, PGC 28887 and UGC 3960) that are fast rotators within $R_c/2$ but slow rotators at $1 R_c$ and Arnold et al. (2014) reported on galaxies that are fast rotators at $1 R_c$ but slow rotators at $2 R_c$ and beyond. These are ES galaxies.

ES galaxies are likely a bridging population between the (once and perhaps still) dust-rich high-mass S0 and the E galaxies. They are not E nor S0 galaxies; similarly, they cannot be binned as either a slow or a fast rotator. To better help distinguish them from E galaxies, Graham et al. (2016b) introduced the term ellicular to capture their halfway nature between ‘elliptical’ and ‘lenticular’ galaxies.³ Here, the $M_{\text{bh}}-M_{\star}$ diagram is explored for signs of displacement between ES and (non-BCG) E galaxies. In the process, the kinematics, morphology and light profiles of the ES and E galaxies were revisited. This has led to some interesting observations into the nature of (evolving) galaxy light profiles and, thus, galaxy components. In particular, an explanation for, and the connection between, embedded and anti-truncated discs is offered. Furthermore, the dynamical heating of discs and the effective erosion or camouflage(?) of their exponential density profile is regarded as leading to the production of Sérsic (1963) $R^{1/n}$ light profiles, whose mathematical properties are reviewed in Graham & Driver (2005).

The data for this investigation are mentioned in Section 2, where a case study of NGC 3379 is presented. This galaxy was not only long-regraded as an E galaxy (Hubble 1926) but as an exemplification of the standard light profile (de Vaucouleurs & Capaccioli 1979) for de Vaucouleurs’ (1953) $R^{1/4}$ model.⁴ Here, it is

³ They appear closer to E than S0 galaxies and, in past literature, were more commonly designated E than S0, hence the preference for the name ellicular over lenticular.

⁴ Sérsic (1968) developed the generalised $R^{1/n}$ model to broadly describe

revealed that the fast rotating galaxy NGC 3379 likely has two stellar discs, reflective of its merger origin. Appendix A provides new galaxy decompositions for additional ETGs and a collective insight from their light profiles. In particular, it is revealed that the single $R^{1/n}$ model of ETGs is likely accounting for a bulge plus a combination of (dynamically-heated) discs. It is suggested here that this mixing leads to the Sérsicification of galaxy light profiles. To illustrate this, an analysis of three additional S0 galaxy light profiles is presented in Appendix A, along with a pair of ES galaxy profiles, a pair of E galaxy profiles, and one E BCG profile. Patterns emerge that support the successive merger origin of these galaxies. All light profiles and magnitudes herein are calibrated to the AB rather than the Vega magnitude system. The results of regression analyses between M_{bh} and $M_{\star, \text{sph}}$ (and $M_{\star, \text{gal}}$) are presented in Section 3, and a discussion is provided in Section 4, along with connections to other elliptical/spheroid-like galaxies, namely compact elliptical (cE) and ultra-compact dwarf (UCD) galaxies.

2 DATA

2.1 Sample

Graham & Sahu (2023a) tabulate spheroid (and galaxy) stellar masses for a sample of ~ 100 galaxies with directly measured black hole masses. The galaxy sample has been uniformly imaged at $3.6 \mu\text{m}$ with the Infrared Array Camera - channel 1 (IRAC-1: Fazio et al. 2004) aboard the *Spitzer Space Telescope* (Werner et al. 2004) and quantified with multi-component decompositions of the light. As described in Sahu et al. (2019a), roughly half of the galaxy sample were analysed using images provided by the Spitzer Survey of Stellar Structure in Galaxies (S⁴G: Sheth et al. 2010; S4G team 2015) project⁵, with the remainder analysed by either mosaicking Spitzer images, as described in Savorgnan & Graham (2016), or studying images taken from the Spitzer Heritage Archive (SHA: Wu et al. 2010).⁶ The SHA has a smaller effective pixel scale of 0.60 arcseconds, and thus a different photometric zero-point of 21.581 mag.⁷ Post Basic Calibrated Data (pbcd, aka level 2) image mosaics (maic.fits files) were used from the SHA.

In the current investigation, the subsamples of E and ES galaxies are studied more closely. In the past, and still today, ES galaxies tend to be grouped with E galaxies. Although Graham & Sahu (2023b) recognised the ES galaxies as something of a halfway station between E and S0 galaxies, the ES galaxies were intentionally grouped with the E galaxies in Graham & Sahu (2023a) and for the regression analysis in Graham (2023c). That sample of ES and E galaxies excluded the ten BCGs (from the parent sample of ~ 100 galaxies), nine of which reside to the right of (not on) the quadratic $M_{\text{bh}}-M_{\star}$ relation defined by the E and ES,e galaxies⁸, as expected if BCGs are, on average, built from the merger of E and/or ES,e galaxies. Brightest group galaxies (BGGs) and non-E

BCG, of which there were just two, are generally not expected to have experienced the same level of mergers as E BCG. This previous grouping of ES,e and non-BCG E galaxies was done because it was considered too much to introduce/discuss their separation in that study. The author also suspected that a couple of the E galaxies may have been misidentified ES (or S0) galaxies. This has been investigated here with recourse to kinematic data to inform the galaxy decompositions further. The light profiles of four S0 and 1 ES,e galaxies requiring the addition of a (previously missed) disc are presented here, and new spheroid (stellar) masses are derived. Four additional galaxies (2 E, 1 ES,e, and 1 E BCG) have their light profile presented and analysed here, and a slightly improved model is obtained due in part to the inclusion of data at smaller ($\lesssim 5''$) and larger radii than used before.

Table 1 lists the sample of non-BCG E and ES,e galaxies, along with a reference to where each galaxy's decomposition can be found and notes regarding their kinematics. Spheroid and galaxy stellar masses (based on a *Salpeter* IMF Graham & Sahu 2024) are also provided there, along with the galaxies' central black hole masses taken from Graham & Sahu (2023a). For the forthcoming investigation of the M_{bh}/M_{\star} diagram, these E and ES,e galaxies are now regarded as two separate populations.

2.2 ES,e galaxies

As noted above, ES galaxies, including many 'disc ellipticals' (Nieto et al. 1988; Capaccioli & Vietri 1988; Michard & Simien 1988), have tended to be grouped with the E galaxies, and this convention was used in Graham & Sahu (2023a). However, the ES,e (and ES,b) galaxies in Graham & Sahu (2023a) had been modelled as bulge+disc systems, and half of these were previously identified as such by Nieto et al. (1988). The present sample's ES,e galaxies are NGC 821, NGC 1275 (BCG in the Perseus Cluster), NGC 3377, NGC 3414, NGC 3585, NGC 3607 (recognised by Krajnović et al. (2011) as having a fast embedded disc within a slower disc), NGC 4473 (Emsellem et al. 2011, counter-rotating stars, '2 σ galaxy'), NGC 4552 (aka M89; BGG in NGC 4552 Group of 12 within the Virgo B Cluster), NGC 4621 (a prototype E galaxy in Hubble 1926), and NGC 4697 (BGG in NGC 4697 Group of 37). Further details are provided in Table 1.

Läsaker et al. (2014) had four of the above galaxies in their sample and modelled NGC 821, NGC 3377, and NGC 4697 with a thin embedded disc, missing only the disc in the galaxy NGC 4473, which they classed as an E galaxy. The embedded discs in NGC 821, NGC 3377, and NGC 4473 are evident in these galaxies' modified/local stellar spin profiles (Bellstedt et al. 2017b, their figure 2). Läsaker et al. (2014) additionally regarded NGC 3115 and NGC 4342 (van den Bosch et al. 1998) — from the larger sample of ~ 100 galaxies — as having embedded discs contributing ~ 10 per cent of the total flux. NGC 4342 was modelled with an embedded disc in Sahu et al. (2019a) but is problematic due to the galaxy's stripped nature. It is, therefore, not included in the current ES,e galaxy data set. As in Graham & Sahu (2023b), NGC 3115 is also considered an ES galaxy with an embedded disc, but it is a compact ES,b galaxy (like Mrk 1216, NGC 1271 and NGC 1277, NGC 1332, NGC 5845 and NGC 6861) and therefore it is included with the (merger-built) dust-rich S0 galaxies because it is more like the *bulge* of a massive S0 galaxy. In the literature, such ES,b galaxies have tended to be grouped with the S0 galaxies, which was done by Graham & Sahu (2023a) for the four ES,b galaxies identified there. These are excluded from the ES,e sample.

galaxies that he thought had an $R^{1/4}$ -bulge and an exponential disc. If no disc was present, it was assumed the $R^{1/n}$ model would default to the $R^{1/4}$ functional form. From the get-go, the $R^{1/n}$ model was designed to accommodate the presence of an outer disc in S and S0 galaxies. In the latter decades of the 1900s, this model was referred to as the $R^{1/4}$ 'law' as it had become so ingrained as a mainstay of galaxy structure.

⁵ <https://irsa.ipac.caltech.edu/data/SPITZER/S4G/>

⁶ <https://irsa.ipac.caltech.edu/applications/Spitzer/SHA/>

⁷ The zero-point is $21.097 + 2.5 \log(0.75/0.60)^2 = 21.581$.

⁸ The notation ES,e is used for those ES galaxies more akin to (extended) E galaxies.

4 *Graham*

Table 1. ES and E galaxy sample

Galaxy	$\log(M_{\text{bh}}/M_{\odot})$	$\log(M_{\star,\text{sph}}/M_{\odot})$	$\log(M_{\star,\text{gal}}/M_{\odot})$	(Source of decomposition). Kinematic notes
(10 – 1 S0 + 1 former ES =) 10 ES,e galaxies				
NGC 0821	7.59±0.17	10.84±0.15	10.90±0.14	(GS23). Regular (fast) rotator within $\approx 1 R_e$ (E+11, K+11, B+17). Misaligned rotation at larger radii (Coccatto et al. 2009; Teodorescu et al. 2010; Schauer et al. 2014).
NGC 1275	8.88±0.21	11.56±0.18	11.60±0.17	(SGD19). BCG/cD in Perseus Cluster with KDC and undigested component.
NGC 3377	7.89±0.03	10.30±0.14	10.36±0.13	Merger (Conselice et al. 2001). $V/\sigma = 48/246 = 0.20$ (Heckman et al. 1985).
NGC 3414	8.38±0.09	10.95±0.19	10.98±0.18	(GS23). Regular (fast) rotator (E+11, K+11, B+17). Twist in direction of rotation at larger radii (Coccatto et al. 2009). Possible merger (Nykytyuk 2015).
NGC 3585	8.49±0.13	11.38±0.15	11.39±0.14	(SG16). Nuclear disc, counter-rotating core (K+11) gives illusion of slow rotation.
NGC 3607	8.16±0.18	11.29±0.18	11.37±0.17	Polar ring (Whitmore et al. 1990). Merger (Jog & Maybhate 2006).
NGC 4291	8.51±0.37	10.68±0.19	10.72±0.18	(SG16). High-rotation (Scorza & Bender 1995a).
NGC 4473	8.07±0.36	10.75±0.13	10.83±0.13	(This work). Regular (fast) rotator (E+11, K+11). Merger (Rickes et al. 2009a).
NGC 4552	8.67±0.05	11.01±0.16	11.07±0.16	(This work). $V/\sigma = 68/278 = 0.24$ (Bender et al. 1994). Previously E galaxy.
				(SG16). Fast rotator (E+11, B+17). Counter-rotating inner discs (K+11).
				(SGD19). Non-regular (slow) rotator (K+11). Twisted isovelocity contours (E+11).
				Disc with inner ring and undigested component. Shells. (Malin & Carter 1983).
				Disc with inner ring and undigested component. Shells. (Malin & Carter 1983).
NGC 4621	8.59±0.06	11.24±0.16	11.28±0.15	BGG in NGC 4552 Group. Well on its way to becoming an E galaxy.
				(SG16). Regular (fast) rotator (E+11, K+11). Rare prolate kinematics.
(17 – 3 S0 – 1 ES =) 13 non-BCG E galaxies				
IC 1459	9.38±0.20	11.69±0.17	11.69±0.17	(SG16). Counter-rotating core or discs (Franx & Illingworth 1988)
				(Prichard et al. 2019). $V/\sigma = 40/302 = 0.13$ (Franx et al. 1989). Ionised gas disc with spiral pattern (Goudfrooij et al. 1990). Shells (Forbes et al. 1995).
NGC 1407	9.65±0.08	11.60±0.17	11.66±0.16	(SGD19). KDC. Merger and slow rotator (B+17).
				(Schauer et al. 2014; Johnston et al. 2018).
NGC 1600	10.25±0.04	12.06±0.13	12.06±0.13	(SGD19). $V/\sigma = 7/312 = 0.02$ (Bender et al. 1994). Possible merger.
NGC 3608	8.30±0.17	10.98±0.14	10.98±0.14	Shells (Forbes & Thomson 1992; Matthias & Gerhard 1999).
NGC 3923	9.47±0.13	11.55±0.17	11.55±0.17	(SG16). Slow rotator (E+11, B+17). Counter-rotating core (K+11). Marginally misaligned phot./kin. axis. Shells. (Forbes & Thomson 1992; Coccatto et al. 2009).
NGC 4261	9.20±0.09	11.52±0.16	11.54±0.15	(SGD19). Slow rotator (Pellegrini et al. 1997). Merger. Shells (Prieur 1988),
NGC 4374	8.95±0.05	11.61±0.15	11.61±0.15	(Zepf et al. 1995; Bílek et al. 2016).
NGC 5077	8.85±0.23	11.27±0.21	11.37±0.20	(SG16). Non-regular slow rotator (E+11, K+11). Twisted isovelocity contours (E+11). Past mergers (Bonfini et al. 2012; D’Abrusco et al. 2013).
NGC 5576	8.19±0.10	10.90±0.16	10.90±0.16	(SG16). Non-regular slow rotator (E+11, K+11, B+17). Misaligned phot./kin. axis (Coccatto et al. 2009). Many(?) mergers (Gómez & Richtler 2004; Yoon et al. 2013).
NGC 5846	9.04±0.06	11.55±0.15	11.55±0.15	(This work). KDC, ring, and accreted gas/dust disc. (Raimundo 2021).
NGC 6251	8.77±0.16	11.80±0.16	11.84±0.15	Possible ES,e galaxy.
NGC 7052	9.35±0.05	11.46±0.13	11.46±0.13	(SG16). Non-regular slow rotator (E+11, K+11).
NGC 7619	9.36±0.09	11.69±0.14	11.71±0.13	(SG16). Non-regular slow rotator (K+11, B+17). Marginally misaligned phot./kin. axis (Coccatto et al. 2009). Filamentary dust (Forbes et al. 1997).
				(This work). $V/\sigma = 40/293 = 0.14$ (Heckman et al. 1985);
				$V/\sigma = 54/288 = 0.19$ (Busarello et al. 1992). Dust lane (Nieto et al. 1983).
				(SGD19). $V/\sigma = 40/270 = 0.15$ (Wagner et al. 1988).
				(SG16). Regular borderline-slow rotator [†] , $V/\sigma = 0.16$ (Loubser et al. 2022).
4 (previously classified E and ES,e) S0 galaxies				
NGC 4697	8.26±0.04	10.20±0.16	10.86±0.14	(This Work). Regular (fast) rotator (E+11, K+11, B+17). BGG in NGC 4697 Group.
				Merger (Sambhus et al. 2006; Spiniello et al. 2015). Possible ES,e galaxy
NGC 3091	9.62±0.08	11.25±0.22	11.70±0.20	(This work). $V/\sigma = 71/286$ (Franx et al. 1989); $V/\sigma = 96/259$ (Busarello et al. 1992).
NGC 3379	8.62±0.13	10.27±0.20	10.89±0.18	(This work). Regular (fast) rotator $V_{\text{rot}} \gtrsim 83 \text{ km s}^{-1}$ (K+11), Douglas et al. (2007).
NGC 4649	9.66±0.10	10.81±0.16	11.48±0.14	(This work). Regular (fast) rotator $V_{\text{rot}} \gtrsim 114 \text{ km s}^{-1}$ (K+11; B+17), (De Bruyne et al. 2001).
Brightest Cluster Galaxy (E galaxy)				
NGC 4486	9.81±0.06	11.58±0.15	11.58±0.15	(This work). Non-rotating galaxy (K+11).

Black hole masses and most stellar masses are sourced from [Graham & Sahu \(2023a\)](#). References showing decompositions of the galaxy light are SG16 = [Savorgnan & Graham \(2016\)](#), SGD19 = [Sahu et al. \(2019a\)](#), and GS23 = [Graham & Sahu \(2023b\)](#). New spheroid and galaxy stellar masses are provided in ‘This work’ for nine galaxies. Kinematic references: K+11 = [Krajnović et al. \(2011\)](#); E+11 = [Emsellem et al. \(2011\)](#); and B+17 = [Bellstedt et al. \(2017a\)](#). K+11 and E+11 measurements pertain to roughly the inner $1 R_e$, where embedded discs reside. KDC = Kinematically decoupled core. [†]Something seems amiss with the plotting of NGC 7619 in the λ_e -magnitude diagram in [Loubser et al. \(2022, their figure 5\)](#).

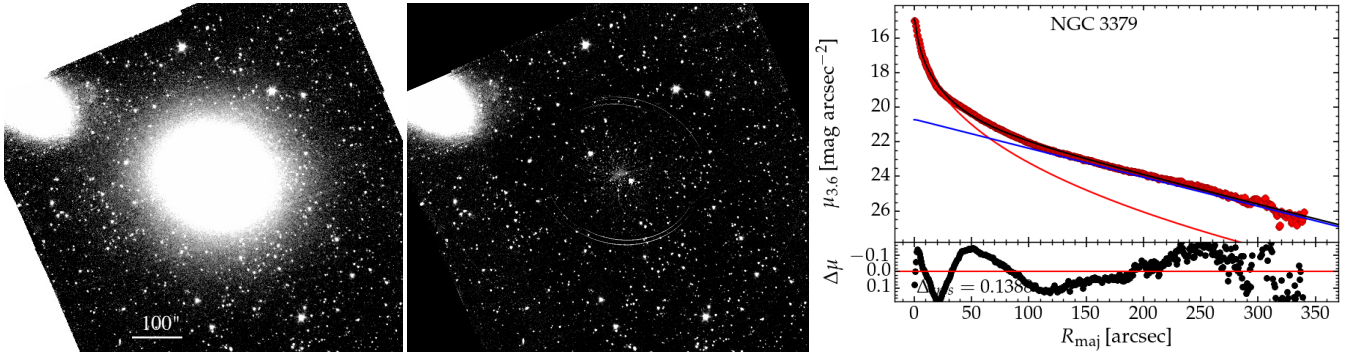


Figure 1. Left: *Spitzer/IRAC1* 3.6 μm image of NGC 3379, courtesy of S⁴G (pipeline 1 image: Muñoz-Mateos et al. 2015). The scale bar is 100'' = 5.3 kpc long. North is up, and east is left. Middle panel: The galaxy light of NGC 3379 and the ‘sky-background’ have been independently determined and subtracted. Right panel: Sérsic spheroid (red curve, $R_{e,\text{maj}} = 20''.9$, $\mu_e = 18.90$ mag arcsec⁻², and $n_{\text{maj}} = 2.74$) and exponential disc (blue line: $\mu_0 = 20.70$ mag arcsec⁻², $h = 65'' = 3.45$ kpc). The disc is also evident in the kinematic map from Krajnović et al. (2011, their figure C1).

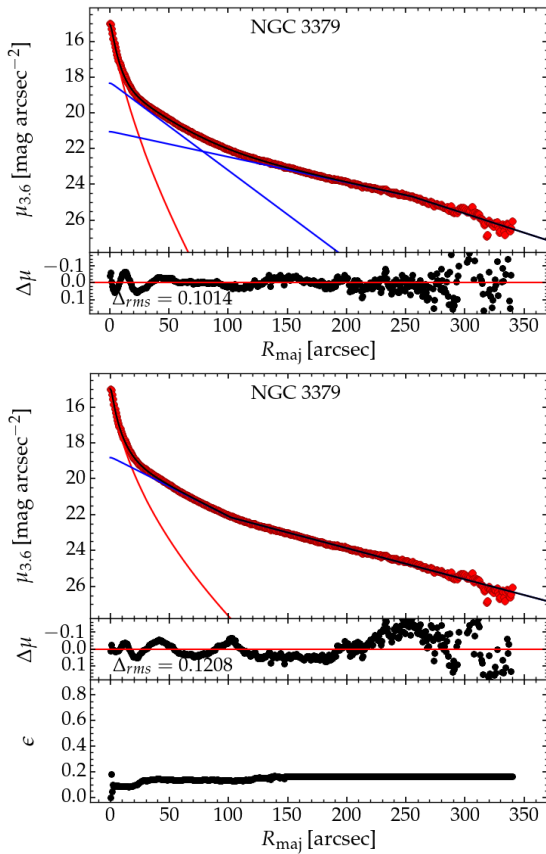


Figure 2. Preferred decompositions for NGC 3379. Top panel: Sérsic spheroid (red curve: $R_{e,\text{maj}} = 6''.4$, $\mu_e = 17.10$ mag arcsec⁻², and $n_{\text{maj}} = 1.44$) plus intermediate-scale disc (straight blue line: $\mu_0 = 18.23$ mag arcsec⁻², $h = 21''.5 = 1.14$ kpc) and weakly-truncated (at $r = 261''$) large-scale disc (bent blue line: $\mu_0 = 20.97$ mag arcsec⁻², $h_{\text{inner}} = 74'' = 3.9$ kpc, $h_{\text{outer}} = 50'' = 2.65$ kpc). Bottom panel: Sérsic spheroid (red curve: $R_{e,\text{maj}} = 8''.5$, $\mu_e = 17.55$ mag arcsec⁻², and $n_{\text{maj}} = 1.87$) plus anti-truncated disc (bent blue line: $\mu_0 = 18.77$ mag arcsec⁻², $R_{\text{bend}} = 102''$, $h_{\text{inner}} = 32''.6 = 1.73$ kpc, $h_{\text{outer}} = 62''.3 = 3.3$ kpc). Note: as seen in the upper panel, an additional downward bend at $r \approx 260''$ would improve the fit in the lower panel.

Graham & Sahu (2023a) and Graham & Sahu (2023b) identified 17 (non-BCG, non-cD) E galaxies, ten suspected ES,e galaxies, and an additional 8 E (plus 1 S0) cD/BCGs. These E and ES,e classifications have been checked via a re-evaluation of the light profiles, with recourse to published kinematic data. Changes are detailed in the following subsection and Appendix A.

2.3 Misclassified ES and S0 galaxies

Stellar discs are often missed in ETGs. This oversight effects studies concerned with galaxy morphology in the $M_{\text{bh}}-M_{\star}$ diagram. For example, if S0 galaxies are modelled as discless E galaxies, this can overestimate the spheroid mass by a typical factor of 4 (Laurikainen et al. 2005). This affects the $M_{\text{bh}}-M_{\star,\text{sph}}$ scaling relations and impacts the reported sizes and densities of the galaxies’ spheroidal component.

Graham & Sahu (2023a) mistakenly regarded NGC 3379 (from Savorgnan & Graham 2016) and NGC 3091 and NGC 4649 (from Sahu et al. 2019a) as E galaxies. This was because additional components, such as discs, were only included in the modelling of the galaxies’ light if convincing evidence was at hand. These three galaxies are remodelled here to reveal their S0 nature better. NGC 4697 (from Savorgnan & Graham 2016) is also remodelled here as an S0 rather than an ES galaxy. However, arguably, the outer thick disc in this galaxy is better regarded as a slowly rotating spheroid, as is the case with, for example, NGC 821 and NGC 3377 (Arnold et al. 2014; Bellstedt et al. 2017b). This is discussed later in regard to the metamorphosis of galaxies. Finally, NGC 4291 (from Savorgnan & Graham 2016) is remodelled as an ES,e galaxy rather than an E galaxy, although the change to the spheroid mass is only 0.12 dex.

The following subsection presents the reanalysis of NGC 3379, while the additional remodelled galaxies are presented in Appendix A to aid readability. Collectively, a double disc structure is revealed for the S0 galaxies that is well captured with an anti-truncated disc model. A double disc structure likely reflects the (e.g. S + S) merger origin of these S0 galaxies. Appendix A also remodels a further four galaxies but does not alter their morphological classification. As shall be seen, the profiles and their decompositions prove to be highly illustrative as to the nature and evolution of ETGs. The evolving nature of the ETG light profiles shown in Appendix A reveals how the double disc structure of massive S0 galaxies gives way to the embedded discs

of ES galaxies and the apparent absence of discs in E galaxies. As seen in Section 3, this picture is accompanied by transitions of galaxy morphology across the $M_{\text{bh}}-M_{\star,\text{sph}}$ diagram.

The revised sample of (17 – 3 S0 – NGC 4291 =) 13 non-(cD/BCG) E galaxies are listed in Table 1 along with (10 + NGC 4291 – NGC 4697 =) 10 ES,e galaxies.

2.3.1 NGC 3379 (M105): double disc or anti-truncated disc

NGC 3379 is supposed to be the personification of the $R^{1/4}$ model (de Vaucouleurs & Capaccioli 1979). Here, it is demonstrated that the light profile of this fast-rotating galaxy (Davis et al. 1985; Krajnović et al. 2011) is best represented by a bulge plus a double-disc, or antitruncated disc, structure.

A 3.6 μm image for NGC 3379 was taken from S⁴G and has a pixel scale of 0.75 arcseconds and a photometric zero-point of 21.097 mag. The Image Reduction and Analysis Facility (IRAF) task ISOFIT (Ciambur 2015), which replaces the flawed ELLIPSE task (Jedrzejewski 1987), was used to extract the major-axis and geometric mean radius, $r = \sqrt{ab}$, light profile, known as the equivalent-axis light profile⁹, while also capturing position angle twists, ellipticity gradients and radially-dependent, higher-order Fourier harmonic terms describing isophotal departures from a pure ellipse. The new IRAF task CMODEL (Ciambur 2015) was used to generate a two-dimensional model of the galaxy that was subtracted from the image. The associated galaxy light profile that accounts for all of this information was modelled with the Python code PROFILER (Ciambur 2016), which can fit multiple components. The result is shown in Fig. 1 when using a traditional Sérsic-bulge plus exponential-disc model.

NGC 3379 is the second brightest galaxy in the M96 (aka Leo I) Group, a group of at least 36 galaxies (Karachentsev et al. 2015), and it is the brightest galaxy in the smaller NGC 3779 Group.¹⁰ It is not optimally modelled in Savorgnan & Graham (2016) due to an overlooked disc (Capaccioli et al. 1991; Statler & Smecker-Hane 1999; Krajnović et al. 2011) with an ellipticity on the sky of just 0.14 (Savorgnan & Graham 2016). Modelling NGC 3379 to nearly six arcminutes (Fig. 1) yields a total (model-extrapolated) apparent magnitude $\mathfrak{M}_{3.6,\text{gal}} = 8.74$ mag and a bulge magnitude $\mathfrak{M}_{3.6,\text{sph}} = 9.31$ mag when including a single, exponential, large-scale disc. This yields a bulge-to-total (B/T) ratio of 0.59. Using a Galactic-extinction-corrected (Schlegel et al. 1998; Schlafly & Finkbeiner 2011) $(B - V)_{\text{Vega}}$ colour of 0.94 mag (RC3; de Vaucouleurs et al. 1991), courtesy of the NASA/IPAC Extragalactic Database¹¹ (NED)¹², gives a (stellar mass)-to-light ratio $M_{\star}/L_{3.6} = 0.80$ (Graham & Sahu 2023a, their equation 4). This is based on a diet-Salpeter IMF (Bell et al. 2003), as are all the stellar masses presented herein. At a luminosity distance of 10.9 ± 1.6 Mpc (Karachentsev et al. 2015), NGC 3379’s total 3.6 μm absolute magnitude $\mathfrak{M}_{3.6,\text{gal}} = -21.45$ mag, and using an absolute magnitude for the Sun of $\mathfrak{M}_{\odot,3.6} = 6.02$ mag (AB; Willmer 2018), the logarithm of the galaxy’s stellar mass is 10.89 ± 0.20 dex. As in Graham & Sahu (2023a), the uncertainty on the mass comes from adding, in

⁹ It is equivalent to a light profile extracted from circularised isophotes, initially with major and minor axis lengths a and b .

¹⁰ Observations have come a long way since the Herschels observed what was GC 2203 (Herschel 1864), now NGC 3379 (Dreyer 1888), with the 30-inch metal reflecting telescope that they purchased in 1793 from the estate of John Michell, who had famously predicted black holes Michell (1784).

¹¹ <https://doi.org/10.26132/NED5>

¹² <https://ned.ipac.caltech.edu/>

quadrature, the uncertainty on the distance, M/L ratio, and magnitude (see equation 9 in Sahu et al. 2019a). As such, the only change in the formal uncertainty discussed in Graham & Sahu (2023a) is the increased uncertainty on the spheroid magnitudes from 0.15 to 0.25 mag. For E galaxies redesignated as ES galaxies, this change is from 0.15 to 0.20 mag. The above galaxy stellar mass is just 0.08 dex smaller than that reported in Graham & Sahu (2023a). However, the spheroid mass fraction of 0.59, which is not yet applied, may still be too high.

In the top panel of Figure 2, a (weakly truncated, down-bending) large-scale disc plus an intermediate-scale exponential disc is used to decompose NGC 3379’s light distribution, along with the Sérsic spheroid function, to improve the fit shown in Fig. 1. This improvement is evidenced by the wholesale removal of the snake-like pattern in the residual light profile seen in Figure 1, whose curvature highlighted a mismatch in form between the model components and the actual galaxy. With the new decomposition, the galaxy’s apparent magnitude remains 8.74 mag while the spheroid mag dims from 9.31 to 10.28 mag. The B/T flux ratio is now 0.24. A remarkably similar outcome is observed with NGC 4649 (Appendix A). Curiously, this B/T ratio of $\sim 1/4$ is typical of S0 galaxies when modelled with bulge+bar+disc components (Laurikainen et al. 2005). The ellipticity profile of NGC 3379 does not suggest a bar is present.

Simulations suggest that NGC 3379 may be a merger remnant, resembling what the Antennae galaxies (NGC 4038/4039) will look like in 3 Gyr from now (Lahén et al. 2018). The presence of two discs (plus spheroid) support the merger origin of this galaxy from the union of two disc galaxies.

While the (potential) detection of two discs is at first a surprising new result for NGC 3379 (and NGC 4649 and others in Appendix A), it should perhaps not be unexpected given that ETGs with double discs are known to exist. Indeed, while some ETGs are known to have two discs, e.g. NGC 4494 (Krajnović et al. 2011; Bellstedt et al. 2017a), sometimes one even counter-rotates with respect to the other, e.g. NGC 4550 (Rix et al. 1992) and NGC 4528 (Krajnović et al. 2011). It is plausible, if not likely, that in NGC 3379 we are witnessing the ongoing reassignment of disc stars into spheroid stars, with an additional dry major merger required to complete the creation of a pure E galaxy. This is in accord with observed galaxy-type-dependent $M_{\text{bh}}/M_{\star,\text{sph}}$ ratios (Graham & Sahu 2023a; Graham 2023c).

The double disc structure in the upper panel of Figure 2 suggests that a single anti-truncated disc model (Pohlen et al. 2002; Erwin et al. 2005) may be applicable, and this is shown in the lower panel of Fig. 2. The transition from bulge to disc at 20–30’’ meshes with the slight jump in the ellipticity profile from 0.09 to 0.13 over this range, and a second slight jump can be seen at 110–140’’ that is associated with the outer disc. The anti-truncated nature of (some) S0 galaxy discs may, therefore, be due to the merging of galaxy discs. This scenario need not be the origin of all anti-truncated discs; indeed, in some S galaxies, a more prosaic explanation is often the occurrence of an outer spiral arm or ring. Although the field-of-view of the frame containing NGC 3379 extends south-west to twice the extent shown in Fig. 1, the change in slope of the light profile at $r \approx 250''$ could conceivably be due to an over-subtraction of the actual ‘sky background’. The upward bend in the light profile of NGC 3379, starting at $r \approx 110''$, is not due to an insufficient subtraction of the ‘sky background’. The ‘sky background’ was measured from the histogram of the image’s pixel values (Almoznino et al. 1993; Davis et al. 2019; Sahu et al. 2019a, see their figure 1).

Three additional S0 galaxies (NGC 3091, NGC 4649,

NGC 4697) are presented in Appendix A. They display the same behaviour in which two apparent discs can be modelled with a single anti-truncated disc. If subsequent merging were to mess up the low-density outer disc — moving stars to higher vertical scale heights and larger orbital radii, expanding the galaxy (e.g. [Gallagher & Ostriker 1972](#)) — but the inner disc was to survive, then these S0 galaxies would be converted into ES galaxies. Erosion of both discs would produce an E galaxy. This sequence and the associated erosion of discs and build-up of the bulge (and bulge-to-disc ratio)¹³ is captured by [Nieto et al. \(1994, their figure 8\)](#)¹⁴ and [Graham \(2024, figure 1\)](#). This is seen in Appendix A, which also presents the light profiles for a couple of ES galaxies (Section A3) and a couple of E galaxies (Section A3) plus one BCG (Section A4).

2.4 Dust

The division between dust-rich and dust-poor galaxies in [Graham \(2023b\)](#) was observed to mirror the galaxies’ underlying origin. Upon investigation of the literature, the bulk of the dust-rich S0 galaxies turned out to be known major wet mergers, while the dust-poor S0 galaxies did not. Consequently, (near and distant) newly-built ETGs can be expected to have dust-dimmed supernovae and partly or wholly obscured AGN as the gas/dust settles towards the galaxy centre.

With time and the growth of galaxy mass comes the tendency to reside in an X-ray hot gas cloud. Residence in such a cloud will destroy a galaxy’s cold gas and dust ([Dwek 1998](#)). A galaxy’s passage through a galaxy-cluster-sized hot gas cloud will also result in ram-pressure stripping of the cold gas and dust from the galaxy. Therefore, not all wet-major-merger-built S0 galaxies are expected to still retain a dust-rich character, and subsequent merger/growth of these galaxies will further their widespread dust loss. As such, the merger-driven evolution from dust-rich S0 galaxy to ES galaxy to E galaxy is expected to result in an apparent brightening of their (Type Ia and other) supernova as the veil of dust thins. Today, while many massive S0 galaxies contain strong dust features, less strong but still widespread dust features can be seen in some E galaxies, e.g., IC 1459, NGC 4374, NGC 5077, and NGC 5846. However, most fully-fledged E galaxies have only a dusty nuclear disc or ring or no dust feature.

It is interesting to explore if the four reclassified E→S0 galaxies contain dust. NGC 3379 (S0) is not dust-rich but has an ~80 pc (radius) nuclear dust ring ([van Dokkum & Franx 1995](#); [Gebhardt et al. 2000](#)), and the bimodal colour distribution of its globular clusters suggests it was formed from hierarchical mergers that produced the red, metal-rich globular clusters ([Rhode & Zepf 2004](#)). NGC 4649 (M60, S0) is also not dusty but is another suspected merger remnant ([D’Abrusco et al. 2014](#)). NGC 3091 (S0) is the BGG in Hickson Compact Group No. 42. Although not dusty, as with NGC 4649, it appears in the X-ray bright catalogue of [Dunn et al. \(2010\)](#), possibly explaining its absence of dust. Finally, NGC 4697 is considered a relaxed merger remnant ([Zezas et al. 2003](#); [Sambhus et al. 2006](#)). It has a nuclear dust disc or ring. Such dusty nuclear discs or rings are a common feature of massive ETGs (e.g. [Jaffe et al. 1994](#); [Rest et al. 2001](#); [Balcells et al. 2007](#)). The

¹³ A caveat is that accretion and non-major mergers might build more disc than bulge.

¹⁴ In [Nieto et al. \(1994\)](#), the ‘hidden discs’ refers to face-on discs rather than intermediate-scale discs.

Table 2. $M_{\text{bh}}-M_{\star,\text{sph}}$ and $M_{\text{bh}}-M_{\star,\text{gal}}$ relations

Galaxy type	N	slope (A)	mid-pt (C)	intercept (B)
$\log(M_{\text{bh}}/M_{\odot}) = A[\log(M_{\star,\text{sph}}/\nu M_{\odot}) - C] + B$ (Fig. 3A)				
S0/Es,b (dust=Y)	18	2.63 ± 0.78	10.70	8.42 ± 0.18
ES,e	10
E (non-BCG)	12	2.03 ± 0.19	11.60	9.39 ± 0.07
BCG	10	2.40 ± 0.40	11.78	9.49 ± 0.13
$\log(M_{\text{bh}}/M_{\odot}) = A[\log(M_{\star,\text{gal}}/\nu M_{\odot}) - C] + B$ (Fig. 3B)				
S0/Es,b (dust=Y)	18	2.82 ± 0.45	11.00	8.14 ± 0.15
ES,e	10
E (non-BCG)	12	2.02 ± 0.21	11.60	9.36 ± 0.06
E (BCG)	08	2.78 ± 0.86	11.78	9.43 ± 0.16

The sample size, N , of each galaxy type, is given in Column 2 and explained in the text. The ν term equals 1.0 here and whenever using stellar mass estimates consistent with those derived from eq. 4 in [Graham & Sahu \(2023a\)](#). Data for the BCG and S0/Es,b (dust=Y) sample, explained in the text, are provided in [Graham & Sahu \(2023a\)](#).

above four galaxies join the S0 galaxies NGC 1023, NGC 4762, and NGC 7332 in that they, too, are mergers that do not display a dust-rich character today.

3 RELATIONS

From the initial sample of ~100 galaxies with directly measured black hole masses and Spitzer 3.6 μm images, there are 13 (= 17–3 S0–1 ES) non-BCG E galaxies (Table 1), 10 ES,e galaxies (including the ES,e/BCG NGC 1275, Table 1) plus an additional 8 E BCG and 1 S0 BCG ([Graham & Sahu 2023b](#), their table 2).

The ‘cleaned’ sample — in the sense that 3 S0 galaxies and 1 ES galaxy have been removed after the new galaxy decompositions performed here — of non-BCG E galaxies define a trend in the $M_{\text{bh}}-M_{\star,\text{sph}}$ diagram (Fig. 3). Excluding only the outlying supergiant E galaxy NGC 6251 — to provide a more robust result — their distribution can be approximated as

$$\log(M_{\text{bh}}/M_{\odot}) = (2.03 \pm 0.19)[\log(M_{\star,\text{sph}}/\nu M_{\odot}) - 11.60] + (9.39 \pm 0.07). \quad (1)$$

This equation is somewhat comparable to the relation for (BCG, E, and ES,e) galaxies without large-scale discs that was discovered by [Sahu et al. \(2019a\)](#) and which has a slope of 1.90 ± 0.20 and an intercept at $\log(M_{\star,\text{sph}}/\nu M_{\odot}) = 11.60$ dex equal to 8.96, albeit based on a constant $M/L_{3.6} = 0.6$ for all ETGs. The $M_{\text{bh}}-M_{\star,\text{gal}}$ diagram and relation for the cleaned sample of non-BCG E galaxies can also be seen in Fig. 3 and Table 2. The result is similar to the $M_{\text{bh}}-M_{\star,\text{sph}}$ relation given that the spheroid contains the bulk, if not the entirety, of the stellar mass in this sample, as can be deduced from Table 1.

The BCG sample is the ten BCGs identified in [Graham & Sahu \(2023b\)](#), while the E (BCG) sample excludes the ES,e BCG NGC 1275 and the S0 BCG NGC 1316. The latter sample was used when deriving the $M_{\text{bh}}-M_{\star,\text{gal}}$ relation (Table 2). Except for NGC 4486, the BCGs are offset to the right of the $M_{\text{bh}}-M_{\star,\text{sph}}$ relation defined by the non-BCG E galaxies (solid line in Fig. 3), as expected from a (mass-doubling) dry major merger of two non-BCG E galaxies. As such, the BCGs are not simply the high-mass end of the non-BCG E galaxy mass-scaling relation. Conversely, with the exception of NGC 6251, the non-BCG E galaxies tend to be offset to the left of the $M_{\text{bh}}-M_{\star,\text{sph}}$ relation defined by the BCGs

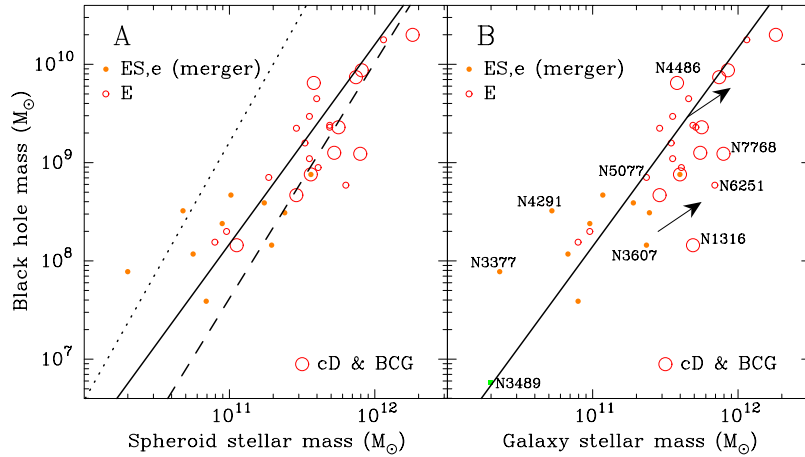


Figure 3. $M_{\text{bh}}-M_{\star,\text{sph}}$ and $M_{\text{bh}}-M_{\star,\text{gal}}$ diagrams and relations for BCG (dashed line), non-BCG E galaxies (solid line), and non-BCG major-merger-built S0 galaxies (dotted line). The arrows show a mass doubling from an equal-mass dry-major-merger, taking galaxies rightward of the steeper than linear $M_{\text{bh}}-M_{\star,\text{gal}}$ relation shown here. (The dust-rich S0 galaxy NGC 3489 happens to reside on the $M_{\text{bh}}-M_{\star,\text{gal}}$ relation defined by the non-BCG E galaxies. A single $M_{\text{bh}}-M_{\star,\text{gal}}$ line for major-merger-built galaxies is provided in [Graham \(2023c\)](#).)

(dashed line in Fig. 3). The BCG with the lowest black hole mass in Fig. 3 is the S0 galaxy NGC 1316 (Fornax Cluster), while the BCG with the third lowest black hole mass is the ES,e galaxy NGC 1275 (Perseus Cluster). The eight other BCGs are E galaxies.

The ES,e galaxies are clearly not drawn from the same population as the non-BCG E galaxies; these discless E galaxies tend to have higher masses, likely reflective of more (substantial) disc-destroying mergers than experienced by the ES,e galaxies. Following [Graham \(2023c\)](#), the regression analysis for the non-BCG major-merger-built S0 galaxies is also shown in Fig. 3, by the dotted line. This sample and the regression line is updated here to include the four reclassified S0 galaxies listed in Table 1. The dust-rich (dust=Y) S0 and ES,b sample of non-BCGs is comprised of the 15 galaxies used in [Graham \(2023c\)](#), minus the BCG NGC 1316 but with the addition of the four S0 galaxies listed in Table 1. The initial sample of 15 galaxies are the 17 listed in table 2 of [Graham \(2023b\)](#) minus NGC 404 ($M_{\text{bh}} \approx 6 \times 10^5 M_{\odot}$; [Davis et al. 2020](#)) and NGC 3489 ([Nowak et al. 2010](#)) due to their elevated weight at the low-mass end of the distribution. At this stage, removing one or two ES,e data points is enough to sway the distribution and, therefore, no reliable relation is derived for this sample. Although a secure regression is not obtained for the ES,e galaxies, their bridging nature between the $M_{\text{bh}}-M_{\star,\text{sph}}$ relations for the major-wet-merger-built S0 galaxies and major-dry-merger-built non-BCG E galaxies is apparent in the left-hand panel of Fig. 3. Among the ES,e galaxies, they tend to have 5–20 per cent of their stellar mass in an intermediate-scale disc, resulting in $\log(M_{\star,\text{gal}}) - \log(M_{\star,\text{sph}}) < 0.1$ dex. As such, there is not a big shift for these galaxies between the $M_{\text{bh}}-M_{\star,\text{sph}}$ and $M_{\text{bh}}-M_{\star,\text{gal}}$ diagrams. The three $M_{\text{bh}}-M_{\star,\text{sph}}$ relations shown in the left-hand panel of Fig. 3 are presented again in Section 4, shown there in relation to black hole scaling relations for other morphological types.

4 DISCUSSION AND INSIGHTS

4.1 Lessons learned from NGC 3379

Several important observations are made below regarding what the remodelled light profile for NGC 3379 is revealing.

Bulge-to-total ratios: The remodelling of NGC 3379 raises the question asked in [Graham & Sahu \(2023b\)](#): What is a bulge? Traditionally, it was defined as the inner excess above the inward extrapolation of the outer disc. However, multicomponent decompositions, such as the inclusion of a bar, can shave the bulge, sometimes considerably so. Furthermore, so can an anti-truncated disc model. Such a model was deemed appropriate for describing NGC 4045 in [Hon et al. \(2022\)](#), reducing the contribution from the bar in that galaxy. While there is often clear evidence for multiple components, such as bars, ansae and rings, counter-rotating discs, and so on, this is not the case for NGC 3379. Therefore, combining the two discs shown in Fig. 2 into a single anti-truncated disc may, for some readers, be more palatable than fitting multiple components beyond a bulge and disc. Eitherway, the use of two discs or an anti-truncated disc reduces the B/T ratio to $\sim 1/4$, down from $\sim 1/2$ when performing a traditional Sérsic-bulge plus exponential-disc fit.

Classical versus pseudobulges: When including a large-scale disc in the modelling of NGC 3379, the Sérsic index of the best-fitting spheroid is reduced from more than 2, specifically 2.74 (Fig. 1), to less than 2 (specifically, 1.44 and 1.87 in Fig. 2). Given NGC 3379 is a wet-merger-built galaxy ([Rhode & Zepf 2004](#)), it has a ‘classical’ bulge, i.e., a merger-built bulge, rather than a pseudobulge built from secular evolution of a single disc. This highlights the problematic nature of (the common practice of) using a bulge’s Sérsic index to dictate the bulge’s origin, a concern raised in [Graham \(2014\)](#) that bulges with $n < 2$ can be built by mergers.

Rotation and dark matter fractions: The assumption that NGC 3379 is dominated by a pressure-supported system would bias attempts to measure the fraction of dark matter in this galaxy. NGC 3379 contains a significant, near-face-on, stellar disc. If the globular cluster and planetary nebula used to probe the kinematics at large radii are also associated with a (somewhat heated) face-on, oblate disc structure (a possibility noted at the end of Section 7.2 in [Douglas et al. 2007](#)), it will lead to a misleading estimate of the required amount of dark matter ([Romanowsky et al. 2003](#)). Given the abundance of dominant large-scale discs in regular and low-mass ETGs, studies using $\sigma^2 R_{\text{e,gal}}/G$, where σ is the stellar velocity dispersion, as a proxy for the dynamical/total mass in these galaxies will typically be in error. This is because the rotation is overlooked

and $R_{e,\text{gal}}$ does not apply to the virial theorem when $R_{e,\text{gal}}$ essentially tracks $R_{e,\text{disc}}$. The subsequent combination of the above mass proxy with the stellar mass to estimate the dark matter fraction is, therefore, expected to be erroneous and misleading for (recognised and unrecognised) S0 galaxies.

Depleted stellar cores: A quantitative reanalysis of partially depleted cores in ETGs with discs will be worth pursuing. The reduced Sérsic index of the bulge model — when a disc component is included in the decomposition — is known to reduce the apparent core break radius, R_b , and stellar mass deficit, M_{def} , of the depleted core relative to the inward extrapolation of the Sérsic model over the core region. This is simply because, with a reduced Sérsic index, the inward extrapolation of the bulge’s revised Sérsic model is not as centrally concentrated and steep. This was the case with the S0 galaxy NGC 4382 (Dullo & Graham 2012), and Dullo & Graham (2014) additionally already note that several other previously misclassified (as E) S0 galaxies may need reinvestigating due to overlooked discs. The core-Sérsic model (Graham et al. 2003; Trujillo et al. 2004) was not employed here due to the 2'' seeing, but it was used in Dullo & Graham (2012) to report $R_b = 1''.03$ for NGC 3379, with Rusli et al. (2013) later reporting $R_b = 1.09 \pm 0.04$ arcsec. The Spitzer 3.6 μm light profile for NGC 3379 was additionally modelled with a core-Sérsic bulge, but this had no significant impact and thus the simpler model was used. If, however, using a routine like GALFIT (Peng et al. 2002) that places maximum weight/trust in the highest signal-to-noise data points, i.e. a galaxy’s centre, then it would be necessary to use the more sophisticated core-Sérsic model (Bonfini 2014) otherwise the results from the Sérsic model would be unduly biased/skewed. Reductions in Sérsic indices may resolve the unexpectedly high $M_{\text{def}}/M_{\text{bh}}$ ratios between 5 and 50 reported for some galaxies while most have ratios less than 4 (Graham 2004; Rusli et al. 2013; Dullo & Graham 2014).

4.2 Galaxy speciation

While widespread dust or a bar is a signpost of a disc in ETGs, for a century, large- and intermediate-scale discs have routinely been missed by visual classification. Careful quantitative studies of images and light profiles, coupled with confirmation from kinematic maps and profiles, has, however, broken this impediment and unlocked great insight into the speciation of galaxies.

Lessons learned from the other remodelled galaxies, when viewed in conjunction with each other, suggest further insights into the structure and speciation of galaxies. Here, the origin of galaxy species is briefly discussed, with insights stemming from careful investigations into their morphology, backed by observations (reported in the literature) of the galaxies’ kinematics and merger history. The typically overlooked population of ES galaxies has been one of the keys to disentangling the wholesale origin of galaxy types. As with discs in S0 galaxies, discs in ES galaxies can be challenging to spot. However, some studies did, and, as noted earlier, these galaxies were referred to as ‘disc ellipticals’ as a point of differentiation (Nieto et al. 1988) from the (pure) E galaxies. Nine examples were provided by Scorza & Bender (1995a), who referred to them as ‘discy ellipticals’, and a dozen examples are displayed in Buta et al. (2015, their figure 23). Arnold et al. (2011) used kinematical information to reveal the (fully embedded) intermediate-scale disc in the ES galaxy NGC 3115 previously presented in Scorza & Bender (1995b, their figure 10b) and later by Buta et al. (2015) and Savorgnan & Graham (2016). Arnold et al. (2014) noted that centrally-fast-rotating ETGs can have rapidly declining (or in-

creasing) specific angular momentum profiles (see also Graham et al. 2017; Bellstedt et al. 2017b). That is, their inner discs may sometimes be embedded in a larger disc.

4.2.1 Mergers versus monolithic collapse

According to a wealth of literature, the sample of dust-rich S0 galaxies with directly measured black hole masses (Graham 2023b, table 2) have been built by mergers. Mergers can build up a spheroid by delivering new stars (from the infalling secondary galaxy) and disrupting pre-existing disc stars (in the primary galaxy). Dry mergers also readily explain the shift to larger spheroids and black hole masses while simultaneously explaining the shift to lower $M_{\text{bh}}/M_{\star,\text{sph}}$ ratios when transitioning from disc-dominated to spheroid-dominated galaxies (Graham & Sahu 2023a). Furthermore, Graham (2023a) reveals that they explain the observed bend in the $M_{\text{bh}}-\sigma$ relation (Graham & Scott 2013; Bogdán et al. 2018; Sahu et al. 2019b). This reduces the role that AGN feedback plays in establishing the black hole scaling relations. Furthermore, Buchner (2024) report a reduced role for AGN feedback in all galaxy types.

Since massive dust-rich S0 galaxies and ES/E galaxies are known merger remnants, it discounts a monolithic collapse scenario (Eggen et al. 1962) for the bulk of their stars. Indeed, as just noted, the $M_{\text{bh}}/M_{\star,\text{sph}}$ ratios of E and ES galaxies are consistent with their creation from the dry merger of massive S0 galaxies. A potential exception worthy of note is that old, metal-poor globular clusters may have formed from a mini/localised collapse, and once they did condense out of a proto-galactic gas cloud, they became effectively collisionless, as was and is the dark matter. While still embedded in a dense gas cloud, dynamical friction and drag will inevitably lead to some of these globular clusters becoming the nuclei of galaxies (Tremaine et al. 1975) around which large gas discs will form and turn into stellar discs, giving rise to the primaeval S0 galaxy population. These nuclei will be returned to in section 4.5.

4.2.2 Accretion and merger driven metamorphosis

Fig. 4 crudely¹⁵ displays the speciation of galaxies, focussing on the spheroid and disc components. The tendency for some discs with longer scalelengths to have fainter central surface brightnesses, i.e. lower densities (Scorza & van den Bosch 1998; Graham 2001), has been incorporated here but is not considered a strict rule. While the major-merger-built galaxies tend to have thick/heated discs (or no discs) which do not endear themselves to bars or spiral patterns, these features can inhabit the precursor population. The demographics of those anatomical features in galaxies across the $M_{\text{bh}}-M_{\star,\text{sph}}$ diagram will be presented in future work. For now, the upper right corner of Fig. 4 includes the ‘Triangal’ from Graham (2023c), developed as an alternative to the ‘Tuning Fork’ (Jeans 1928; Hubble 1936), and the ‘Trident’ or ‘ATLAS^{3D} Comb’ (van den Bergh 1976; Cappellari et al. 2011), which do not have evolutionary arrows, do not recognise the two types of S0 galaxy (primaeval and wet-major-merger-built: Graham 2023b), and have no

¹⁵ This representation is crude in the sense that it does not (yet) incorporate additional features that might be important, such as bar strength, spiral arm strength or winding angle.

direct path linking S galaxy mergers with S0 galaxies. The ‘Triangal’ includes major mergers of both primaevial and wet-major-merger-built (in general, low- and high-mass) S0 galaxies to create ES and E galaxies. This key ingredient was missing from the previous morphology schemata, which did not account for ‘punctuated equilibrium’ events (Graham & Sahu 2023a), such as major mergers of S galaxies. Building on those schemata, the ‘Triangal’ can bypass the gradual changes linking disc galaxies possessing strong spirals (or bars or bulges) to those with weak spirals and then those with no spiral pattern, jumping straight from S to S0, thereby circumventing the limitations of past schema and capturing the major evolutionary pathways. Embellishments of spiral and bar strength will be added in a forthcoming paper.

Among the four remodelled S0 galaxies (Section 2.3.1 and A1) — all of which are considered in the literature to have been built from a major merger event — they appear to have an inner disc with an exponential scalelength of 2 ± 1 kpc and an outer disc with an exponential scalelength of 5 ± 2 kpc. The exception is NGC 3091 in Hickson Compact Group No. 42, with an inner (sole?) disc scalelength of 5 kpc and an outer exponential (halo?) with a scalelength of 15 kpc. Curiously, Seigar et al. (2007) discovered a tendency for halos to have exponential light profiles.

In Fig. 4, one can see how the ‘bulge’ component of S0 galaxies, when defined as the inner excess above the inward extrapolation of the outer exponential profile, will yield a mismatch with the dynamically hot pressure-supported ‘bulge’ (shown by the red curves). The dynamical heating and partial erosion of the outer disc(s) can produce ES galaxies whose disc is fully embedded within what is regarded as a slowly or non-rotating oblate ellipsoid rather than a disc. This situation is seen in kinematic maps that extend beyond $1R_e$ (Arnold et al. 2014).

While de Vaucouleurs et al. (1964) tabulated bright galaxies, noting which were peculiar (‘pec’)¹⁶, Vorontsov-Velyaminov (1959) and Arp (1966) focussed on these peculiar and interacting galaxies. They are transitional types, covering mergers-in-progress, and they encapsulate many recent wet and dry major merger remnants, such as the dust-rich S0 disc galaxies built from gas-rich mergers and E galaxies with stellar shells (e.g. Hansen et al. 1985; Hernquist & Quinn 1988; Xu et al. 2010; Raimundo 2021; Rutherford et al. 2024). Mergers are ‘part and parcel’ of galaxy life and tend to disguise galaxy discs, in part by destroying the spirals (and bars) that would otherwise reveal the presence of these discs. The RC3 (de Vaucouleurs et al. 1991) is full of S0 galaxies that were mislabelled as E galaxies. This is because, from a casual glance at an image, spiral-less galaxy discs tend to resemble spheroids unless they are viewed close to edge-on.

It took kinematic observations (e.g. Graham et al. 1998; Emsellem et al. 2011) to confirm that the actual number of “dynamically hot” galaxies is much lower than was initially thought. Marinoni et al. (1999, their figure 3) showed that (true, slow rotating) E galaxies only dominate the ETG population at magnitudes brighter than $M_{B,Vega} \approx -20.6$ mag ($H_0 = 75$ km s⁻¹ Mpc⁻¹), while S0 galaxies dominate at fainter magnitudes. This was supported by Emsellem et al. (2011) using rotational measures and by Krajnović et al. (2013) using photometric decompositions of the galaxy light. A division at this magnitude had previously been seen between galaxies with and without depleted cores (Faber et al. 1997; Graham & Guzmán 2003), supporting the dominance of dry (gas-poor) galaxy mergers at high masses (e.g. Blanton 2006). The

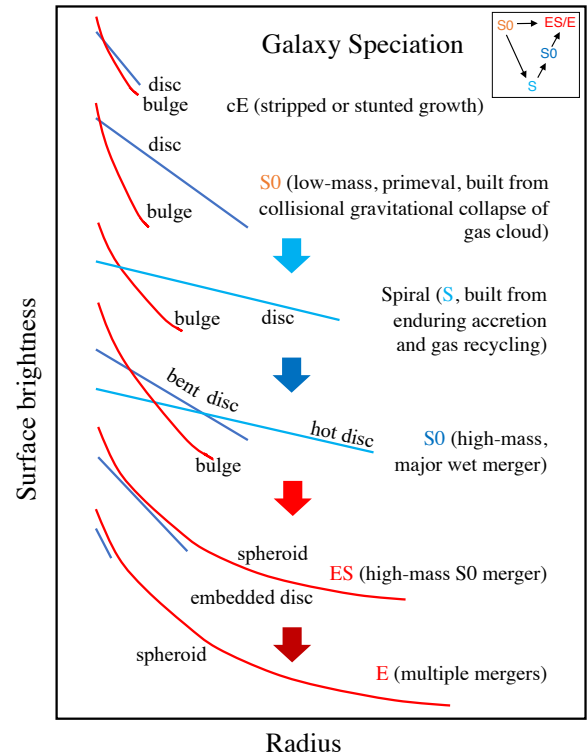


Figure 4. Progressive speciation of common galaxy types, revealing the Sérsicification of galaxy light profiles as Sérsic $n \approx 1$ discs give way to higher- n profiles that decline slowly at large radii. The schematic also helps to visualise/explain the construction of the $R_{e,gal}-n$ relation (Caon et al. 1993; D’Onofrio et al. 1994), the $M_{\star}-n$ relation (Cellone et al. 1994; Young & Currie 1994), and the $M_{bh}-n$ relation (Graham et al. 2001; Graham & Driver 2007). Depleted galaxy cores that can form in dry merger events are not shown. The ‘Triangal’ from Graham (2023c) is shown in the upper-right corner.

scouring action of a binary black hole in a dry merger erodes the central phase-space of stars and leaves its signature as a depleted core (Begelman et al. 1980; Milosavljević & Merritt 2001; Graham 2004; Khan et al. 2013), thereby enabling the identification of galaxies built from gas-poor mergers. The scouring also explains the removal of the dense nuclear star clusters (Bekki & Graham 2010) prevalent in the lower mass galaxies. The prevalence of a central black hole in massive galaxies built from major mergers, such as the black holes found in the BCGs in the upper right of Fig. 5, suggests that the gravitational recoil from colliding black holes (e.g. Campanelli et al. 2007; Baker et al. 2008; Gualandri & Merritt 2008) is, in general, insufficient to remove supermassive black holes from galaxies. Arguably, some black hole binaries that are yet to coalesce — perhaps in a gas-poor spherical galaxy (Berczik et al. 2006; Khan et al. 2013; Vasiliev et al. 2015) — may remain undetected in these galaxies due to the limiting spatial resolution of the kinematic data used to infer the presence of the central mass.

4.2.3 The decline of disc sizes

As noted, S0 galaxies with anti-truncated discs may conceivably arise from the merger of two disc galaxies in which neither disc entirely morphs into a dynamically-hot spheroidal structure. Suppose the outer component becomes sufficiently hot, transitioning

¹⁶ These are often unrelaxed mergers.

from a disc to an ellipsoid, aka spheroid, but the inner, more robust, higher-density disc remains largely intact. In that case, one will have an ES galaxy. The smaller disc outlives the more fragile, and more dispersed, larger disc.

An ES galaxy may also be bolstered by a gas-rich galaxy collision in which the stars experience a non-collisional merger to produce a spheroid. At the same time, the gas and dust undergo a collisional merger. This happens because although the cross-section of a star is much greater than that of a gas particle, the number of gas particles is so vastly higher that gas interactions are much more frequent. Therefore, wet galaxy collisions can ‘heat’ stellar discs to build bulges, while gas and dust form new discs due to gravitational collapse akin to what would have occurred in proto-galaxies building primaeval S0 galaxies. At that time, it was only the dark matter that experienced a non-collisional contraction. Presumably, having experienced a net loss of angular momentum during the disc galaxy collision, the gas collapses to form a smaller disc, adding to the ES nature of the system. Inner gas discs, therefore, need not arise from accretion alone but may also arise out of major mergers.

This process could explain some blue cores in ETGs and some nuclear discs in E galaxies. If nuclear discs in E galaxies arise from the major merger of merger-built S0 galaxies, then it makes sense that, with less gas available in these subsequent collisions and gas shocks robbing it of its angular momentum, the ensuing generation of discs is smaller. These (10s to 100s of pc) nuclear discs may be distinct from, and larger than, the spheroidal-shaped nuclear star clusters seen in low-mass ETGs (e.g. [Graham & Guzmán 2003](#)). One may then expect to find some E galaxies having nuclear discs with stellar populations that are younger than the galaxy at large, e.g. NGC 4261 and NGC 7052. Thus, again, minor accretion events need not be the origin of these discs but rather past (major) mergers. A distinguishing test could be that the heavily recycled gas from mergers is expected to be more metal-rich than the relatively pristine gas brought in from accreted gas clouds.

4.3 Counter rotation

Four galaxies in the sample are known to have counter-rotating components: NGC 3414 (ES,e), NGC 4473 (ES,e, ‘ 2σ galaxy’ [Emmellem et al. 2011](#); [Arnold et al. 2014](#)), IC 1459 (E), and NGC 3608 (E). Although counter rotation could signal the presence of two large-scale discs, and thus it would be interesting to check on a single anti-truncated disc, none of these four galaxies are designated S0 galaxies. They were modelled in [Savorgnan & Graham \(2016\)](#), where NGC 3414 was noted to additionally have a polar ring, as does NGC 5077. While the high ellipticity in NGC 4473, at around 0.4 at $R_{\text{maj}} = 100'' = 7.3$ kpc, is typical of a disc, it has been suggested that this outer ellipticity is the result of multiple minor mergers ([Alabi et al. 2015](#)). However, it perhaps forms a dynamically hot, slowly rotating disc-like structure. The counter-rotation in this galaxy stems from two counter-rotating stellar discs that occupy the inner region ([Krajinović et al. 2011](#)). The fast counter-rotating nuclear disc in IC 1459 contains less than 1 per cent of the galaxy’s total stellar mass ([Franx & Illingworth 1988](#)), and, as such, IC 1459 is not regarded as an ES,e galaxy but instead a slowly rotating E galaxy. Interestingly, IC 1459 also contains a faint large-scale spiral pattern of ionised gas and stars ([Malin 1985](#); [Goudfrooij et al. 1990](#)), and 3 per cent of the stellar population is young (~ 400 Myr [Amblard et al. 2017](#)). Finally, NGC 3608, which resides in a diffuse X-ray halo ([Mulchaey et al. 2003](#)), has a slow ($\lesssim 40$ km s $^{-1}$) counter-rotating core within the inner $\sim 5'' = 0.5$ kpc ([Krajinović et al. 2011](#)). The rise in ellipticity beyond $R_{\text{maj}} \approx 18''$ ([Savorgnan](#)

& [Graham 2016](#)) is associated with the slowly ($\lesssim 40$ km s $^{-1}$) rotating main galaxy ([Arnold et al. 2014](#)). Rather than two discs, this galaxy would likely be well-described by two Sérsic functions, but the author has refrained from performing a double Sérsic fit in the interest of constraining the complexity of the model used here.

4.4 Making waves

Although the sample size is low, the BCG appear to define a near-cubic $M_{\text{bh}}-M_{\star,\text{gal}}$ relation. Their relation’s steep slope (2.78 ± 0.86) is comparable with that seen among the sample of dust-rich S0 galaxies (2.82 ± 0.45), for which there are twice as many, and comparable with the slope of the spiral galaxies (2.68 ± 0.46 : [Davis et al. 2018](#); [Graham 2023c](#), table 1) for which the sample size is three times larger. The dust-poor, low-mass S0 galaxies also appear to follow a distribution in the $M_{\text{bh}}-M_{\star,\text{gal}}$ diagram with a slope steeper than 2 ([Graham 2023c](#), figure A4), although an expanded data set would be valuable to confirm this. These observations beg the question as to whether the near-quadratic $M_{\text{bh}}-M_{\star,\text{gal}}$ relation for the E galaxies underestimates the true slope. Taking the E galaxy scaling $M_{\text{bh}} \propto M_{\star,\text{gal}}^{2.02 \pm 0.21}$ (Table 2), which is very similar to the $M_{\text{bh}} \propto M_{\star,\text{gal}}^{2.07 \pm 0.19}$ scaling for the ensemble of major-merger-built galaxies ([Graham 2023c](#)), and coupling it with the $M_{\text{bh}} \propto \sigma^{8.64 \pm 1.10}$ scaling for massive galaxies with core-Sérsic light profiles likely built from dry major mergers ([Sahu et al. 2019b](#)), one obtains $M_{\star,\text{gal}} \propto \sigma^{4.28}$, which is comparable to the canonical value of 4 for non-dwarf ETGs ([Faber & Jackson 1976](#)).

The Illustris simulation ([Genel et al. 2014](#); [Vogelsberger et al. 2014](#)) has also yielded a quadratic-like distribution in the $M_{\text{bh}}-M_{\star,\text{gal}}$ diagram ([Li et al. 2020](#), their figure 1), see also the MassiveBlack simulated tracks ([Khandai et al. 2012](#), their figure 7), and an array of additional simulations indicating a quadratic or steeper $M_{\text{bh}}-M_{\star,\text{gal}}$ scaling ([Khandai et al. 2012](#); [LaMassa et al. 2013](#); [Bonoli et al. 2014](#)).

Interestingly, as noted above, the low-mass dust-poor S0 galaxies also appear to define their own steep $M_{\text{bh}}-M_{\star,\text{gal}}$ relation (and $M_{\text{bh}}-M_{\star,\text{sph}}$ relation: [Graham 2012](#); [Graham & Scott 2013](#); [Scott et al. 2013](#)), with a notably higher $M_{\text{bh}}/M_{\star,\text{gal}}$ ratio for a given black hole mass than the major-merger-built ETGs. It is postulated that these low-mass galaxies are faded S0 galaxies. In passing, one may speculate if these galaxies are aged counterparts of the tentative ‘blue monsters’ observed at $z > 10$ ([Ziparo et al. 2023](#)). These local S0 galaxies are often overlooked. For instance, their low stellar masses and low-to-zero star formation rates has often resulted in sample selection effects missing many of them in plots of star formation rate versus galaxy stellar mass. Consequently, some tales of galaxy evolution (e.g. [Schawinski et al. 2014](#), and references therein) are incomplete when focussed on the old ideas of making ETGs by either fading S galaxies ([Spitzer & Baade 1951](#); [Gunn & Gott 1972](#)) or colliding S galaxies (e.g., [Toomre 1977](#); [Roos & Norman 1979](#)). Addressing the often overlooked low-mass S0 galaxies that did not form from the above two scenarios has led to the expanded picture of galaxy speciation presented in [Graham et al. \(2024\)](#).

For practical purposes pertaining to studies of gravitational waves from colliding supermassive black holes, which are expected in BCGs and the other major-merger-built galaxies, an $M_{\text{bh}}-M_{\star,\text{gal}}$ relation for merger-built ETGs (dust-rich, high-mass S0 galaxies and ES and E galaxies) is provided in [Graham \(2023c\)](#). The use of $M_{\star,\text{gal}}$ rather than $M_{\star,\text{sph}}$ should be helpful for studies and simulations that do not separate galaxies into bulge/disc components. Ex-

cluding the S and above mentioned faded/preserved dust-poor, low-mass (primordial) S0 galaxies that have not experienced much/any major merger action yielded a slope of ~ 2 rather than ~ 1 for this $M_{\text{bh}}-M_{\star,\text{gal}}$ relation. This relation is not updated here because the reclassification of five galaxies does not change the major-merger-built sample. There are revised $M_{\star,\text{gal}}$ values for nine galaxies, but the changes are not large enough to warrant a rederivation of the $M_{\text{bh}}-M_{\star,\text{gal}}$ relation.

4.5 Compact elliptical (cE) and ultracompact dwarf (UCD) galaxies

This paper has focussed on ETGs that are intrinsically large and luminous, having been built by mergers. There are, however, a couple of types of lower-mass elliptical-like galaxies. These are the rare compact elliptical (cE) galaxies that can form from tidal stripping (Bekki et al. 2001; Graham 2002) and UCD galaxies that can form from even more extreme tidal threshing (Bekki & Freeman 2003; Ideta & Makino 2004; Chilingarian & Mamon 2008; Koch et al. 2012; Pfeffer & Baumgardt 2013; Paudel et al. 2023). The cE galaxies tend to be overly metal-rich for their luminosity (e.g. Chilingarian et al. 2009; Price et al. 2009) and underluminous for their (red) colour (e.g. Graham & Soria 2019, their Figure 11, and references therein), which is as expected if they had previously evolved to a larger mass that was then pared back.

Instead of experiencing tidal stripping, one may ask if some dwarf cE galaxies were instead denied growth due to a hungry, more dominant neighbour or simply a lack of fuel in a void-like environment. Such a mechanism for dwarfism, i.e. born that way, as suggested in Graham (2013, footnote 20) for some cE galaxies, implies that some evolutionary arrows flow to the left *and* right in Fig. 5. This leads to the notion that perhaps some UCDs also need not be the compact nuclei of threshed disc galaxies. Indeed, the similarity of UCDs to large old globular clusters (GCs) has long been noted. Strongly stunted growth in the early Universe might ‘freeze-in’ GC and some UCD galaxies around bigger galaxies. Speculatively, some may have condensed out of proto-galactic gas clouds while the remaining gas continued to experience collisional contraction, forming the main galaxy disc and thus no longer providing gas drag in either the galaxy halo, to drive the GCs/UCDs inwards, or within the GCs/UCDs, to aid runaway collisions and massive black hole growth. Irrespective of this possibility, if galaxies start life by growing a cluster of stars around a massive black hole — with their larger-scale disc subsequently forming — then today’s NSCs and UCDs may be a better comparison point for the high- z AGN referred to as ‘little red dots’ (Labbe et al. 2023; Maiolino et al. 2024) than today’s more fully-formed galaxies.¹⁷

Stepping things back even further, in terms of increased $M_{\text{bh}}/M_{\star,\text{sph}}$ ratios, leads to massive black holes with no stellar association in Fig. 5. Massive naked black holes might form from the direct collapse of giant gas clouds (Doroshkevich et al. 1967; Umemura et al. 1993) or through other mechanisms involving baryons that may have created heavy black hole seeds, such as dark stars and Pop III.1 stars (Spolyar et al. 2009; Banik et al. 2019; Singh et al. 2023). If some black holes instead formed in the first few seconds of the Universe, they would contribute to the ‘dark matter’ of the Universe. Although black hole masses of $10^{5\pm 2} M_{\odot}$

are greater than the theorised primordial black hole population (Argyres et al. 1998; Bean & Magueijo 2002; Villanueva-Domingo et al. 2021), lower-mass primordial black holes could still help to later create heavy ‘seed masses’ for establishing the high- z quasars with virial masses of $10^{8\pm 1}$ (Liu & Bromm 2022; Yuan et al. 2023). The cosmic X-ray background and the cosmic radio background does, however, place limiting constraints on the numbers of 1-1000 M_{\odot} primordial black holes (Ziparo et al. 2022). Nonetheless, at least some dark matter might be ‘black matter’ as these black holes need not be made of baryonic matter.¹⁸

Many globular clusters are old. If giant globulars form early enough while still immersed in a soup of gas, then the gas drag force may lead to runaway collisions and the formation of an IMBH within the system (Zel’dovich & Podurets 1965; Shapiro & Teukolsky 1985). The existence of massive Pop III stars (Schwarzschild & Spitzer 1953) may aid this process (Umeda & Nomoto 2003; Fraser et al. 2017), although the lack of robust IMBH detections in globular clusters currently disfavors this mechanism.

The total collapse of a globular would lead to a naked black hole. On the other hand, if some stars remain in the most massive globulars, one may observe a black hole as the nucleus of a UCD galaxy. If the black hole becomes active and manages to sufficiently blow away the gas causing the drag on the stars, this may act to stabilise the system. Such black hole birth in a dense cluster of stars, a kind of embryonic giant globular (EGG), would not resolve the need for dark matter to explain early structure formation, as these clusters would be baryonic and not start to collapse until after the epoch of recombination, some 380,000 years after the Big Bang (Planck Collaboration et al. 2020). If an EGG or three were to fall into a low-mass, disc-dominated galaxy, the system might well join the black hole galaxy scaling relation.¹⁹ Interestingly, this may be occurring in NGC 4424, with the capture of ‘Nikhuli’ (Graham et al. 2021). This seeding phenomenon is labelled in Fig. 5. On the other hand, if an EGG continues to grow a disc at high- z , the system will likely evolve into a nucleated dwarf ETG, specifically a dwarf S0 galaxy, which are common in galaxy clusters today (e.g. Sandage et al. 1985; Graham & Guzmán 2003).

4.6 A word on entropy

In the Introduction section, entropy was briefly noted in passing. As Bekenstein (1973) proposed, massive black holes have a huge amount of entropy. As black holes become more massive, their surface area grows and their entropy increases. Entropy requires black holes to have a temperature and thus that they radiate, which Hawking (1975) later proved following discussions by Vladimir Gribov and Yakov Zel’dovich in 1972-1973 (Ansel’m et al. 1998; Azimov 2016). The stellar component of galaxies also has a kind of entropy. When the large primordial (collisional) gas clouds contracted, they spun up to conserve angular momentum and formed discs that were supported from further gravitational collapse by their rotation. These are expected to be the first galaxies, some of which may be today’s low-mass, dust-poor S0 galaxies. The

¹⁸ It would take one million $10^6 M_{\odot}$ black holes to account for the missing mass in a (Milky Way)-sized galaxy. Although this is 10^4 times higher than the number of globular clusters, these black holes would still have a sufficiently low volume (and surface) number density to make it unlikely that current gravitational lensing studies in our Galaxy or the Magellanic Clouds would have detected them (Alcock et al. 2000, 2001; Tisserand et al. 2007).

¹⁹ The high scatter for S galaxies in the $M_{\text{bh}}-\sigma$ diagram (Sahu et al. 2019b) might be related to this.

¹⁷ The author publicised this point at August 2024 conferences: <http://cosmicorigins.space/smbh-sexten> and <https://indico.ict.inaf.it/event/2784/>

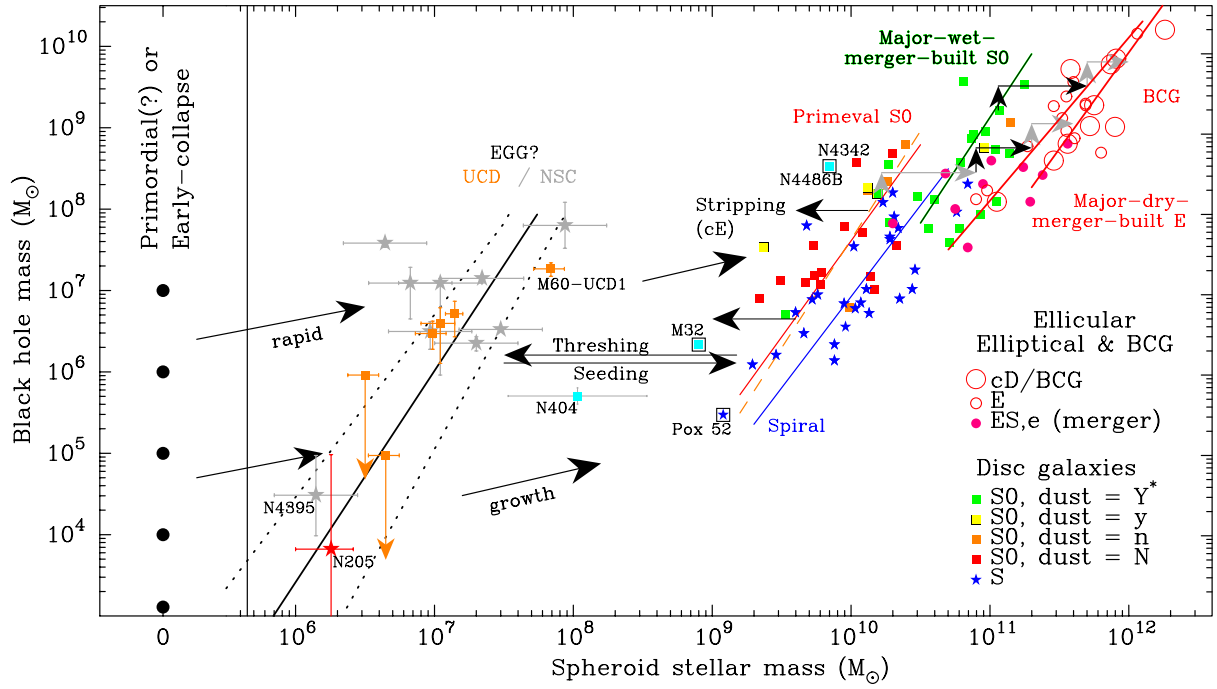


Figure 5. Adaption of figure 6 from [Graham & Sahu \(2023b\)](#), incorporating figure 2 from [Graham \(2020\)](#) for the nuclear star clusters (NSCs) and ultracompact dwarf (UCD) galaxies plus an updated version of figure 1 from [Graham \(2023c\)](#) based on the remodelled galaxies presented herein. * Four merger-built but non-dust-rich galaxies remodelled and reclassified as S0 galaxies (see Table 1) are coded green here as they were grouped with the dust-rich S0 galaxies for the regression. Some low-mass, dust-poor S0 galaxies may be regarded as ancients or elders, representing the disc-dominated galaxies before a spiral pattern was established. The UCD galaxies may be the NSCs of threshed (heavily stripped) disc galaxies or old embryonic giant globulars (EGGs) that partially collapsed to form a central massive black hole. Some of these EGGs may never grow a fully-fledged galaxy around them, or be accreted (at early or late times) into a galaxy and effectively seed it with a massive black hole.

gas cooled within these discs and formed stars (collisionless particles). Repeated major collisions built subsequent generations of galaxies by dynamically heating the discs and building the bulges, thereby more fully filling the phase space of a galaxy’s halo and thus increasing the entropy: chaos over order; ‘hot’ pressure supported spheroids (random orbits) over dynamically-cold rotation-supported discs (ordered orbits).

ACKNOWLEDGEMENTS

This paper is dedicated to the memory of Tom Jarrett (1963-2024). I am blessed to have recently enjoyed Tom’s friendship and passion for astronomy. Tom alerted me to the disc in NGC 4649, which prompted me to re-check the E and ES galaxies in my sample. This reassessment resulted in this paper’s appendix and contributed to the conclusions.

I thank Ewan Cameron for his ongoing support of his R statistical software. I am grateful to David Liptai, Conrad Chan and Robin Humble of the Astronomy Data and Computing Services (ADACS) in Australia for keeping the Image Reduction and Analysis Facility (IRAF) alive on the OzSTAR and ‘Ngarrgu Tindebeek’ supercomputer at Swinburne University of Technology.

Publication costs were funded through the 82783405 Australia and New Zealand Institutions (Council of Australian University Librarians affiliated) Open Access Agreement. Some of this work was performed on the OzSTAR national facility at Swinburne University of Technology. The OzSTAR program receives funding in part from the Astronomy National Collaborative Research Infras-

tructure Strategy (NCRIS) allocation provided by the Australian Government and the Victorian Higher Education State Investment Fund (VHESIF) provided by the Victorian Government. This work has used the NASA/IPAC Infrared Science Archive (IRSA) and the NASA/IPAC Extragalactic Database (NED)²⁰, funded by NASA and operated by the California Institute of Technology. This research has also used the SAO Astrophysics Data System Bibliographic Services and the RSTAN package available at <https://mc-stan.org/>.

5 DATA AVAILABILITY

The imaging data underlying this article are available in the NASA/IPAC Infrared Science Archive.²¹ The S⁴G dataset Digital Object Identifier (DOI) is 10.26131/IRSA425. The spheroid and galaxy stellar masses are tabulated in [Graham & Sahu \(2023a\)](#), with revisions (This Work) in Table 1.

<https://doi.org/10.26131/IRSA425>

REFERENCES

- Agazie G., et al., 2024, *ApJ*, 966, 105
 Alabi A. B., et al., 2015, *MNRAS*, 452, 2208
 Alcock C., et al., 2000, *ApJ*, 542, 281

²⁰ <https://doi.org/10.26132/NED1>

²¹ <https://irsa.ipac.caltech.edu/applications/Spitzer/SHA>

- Alcock C., et al., 2001, *ApJ*, **550**, L169
- Almoznino E., Loinger F., Brosch N., 1993, *MNRAS*, **265**, 641
- Amaro-Seoane P., et al., 2023, *Living Reviews in Relativity*, **26**, 2
- Amblard A., Temi P., Gaspari M., Brighenti F., 2017, *ApJ*, **834**, 20
- Ansel'm A. A., et al., 1998, *Uspekhi Fizicheskikh Nauk*, **41**, 407
- Argyres P. C., Dimopoulos S., March-Russell J., 1998, *Physics Letters B*, **441**, 96
- Arnold J. A., Romanowsky A. J., Brodie J. P., Chomiuk L., Spitler L. R., Strader J., Benson A. J., Forbes D. A., 2011, *ApJ*, **736**, L26
- Arnold J. A., et al., 2014, *ApJ*, **791**, 80
- Arp H., 1966, *ApJS*, **14**, 1
- Azimov Y. I., 2016, in Dokshitzer Yuri L. e. a., ed., Proceedings, Gribov-85 Memorial Workshop on Theoretical Physics of XXI Century : Chernogolovka, Russia, June 7-20, 2015. World Scientific Publishing, pp 9–15 ([arXiv:1608.05727](https://arxiv.org/abs/1608.05727)), doi:10.1142/9789813141704_0004
- Baker J. G., Boggs W. D., Centrella J., Kelly B. J., McWilliams S. T., Miller M. C., van Meter J. R., 2008, *ApJ*, **682**, L29
- Balcells M., Graham A. W., Peletier R. F., 2007, *ApJ*, **665**, 1084
- Banik N., Tan J. C., Monaco P., 2019, *MNRAS*, **483**, 3592
- Banik I., Thies I., Truelove R., Candlish G., Famaey B., Pawlowski M. S., Iбата R., Kroupa P., 2022, *MNRAS*, **513**, 129
- Bean R., Magueijo J., 2002, *Phys. Rev. D*, **66**, 063505
- Begelman M. C., Blandford R. D., Rees M. J., 1980, *Nature*, **287**, 307
- Bekenstein J. D., 1973, *Phys. Rev. D*, **7**, 2333
- Bekki K., Freeman K. C., 2003, *MNRAS*, **346**, L11
- Bekki K., Graham A. W., 2010, *ApJ*, **714**, L313
- Bekki K., Couch W. J., Drinkwater M. J., Gregg M. D., 2001, *ApJ*, **557**, L39
- Bell E. F., McIntosh D. H., Katz N., Weinberg M. D., 2003, *ApJS*, **149**, 289
- Bellstedt S., Forbes D. A., Foster C. A., Romanowsky A. J., Brodie J. P., Pastorello N., Alabi A., Villaume A., 2017a, *MNRAS*, **467**, 4540
- Bellstedt S., Graham A. W., Forbes D. A., Romanowsky A. J., Brodie J. P., Strader J., 2017b, *MNRAS*, **470**, 1321
- Bender R., Saglia R. P., Gerhard O. E., 1994, *MNRAS*, **269**, 785
- Benson A. J., Bower R. G., Frenk C. S., Lacey C. G., Baugh C. M., Cole S., 2003, *ApJ*, **599**, 38
- Berczik P., Merritt D., Spurzem R., Bischof H.-P., 2006, *ApJ*, **642**, L21
- Bertola F., Bettoni D., Danziger J., Sadler E., Sparke L., de Zeeuw T., 1991, *ApJ*, **373**, 369
- Bílek M., Cuillandre J. C., Gwyn S., Ebrová I., Bartošková K., Jungwiert B., Jílková L., 2016, *A&A*, **588**, A77
- Biswas P., Wadadekar Y., 2024, [arXiv e-prints](https://arxiv.org/abs/2405.04166), p. [arXiv:2405.04166](https://arxiv.org/abs/2405.04166)
- Blakeslee J. P., Lucey J. R., Tonry J. L., Hudson M. J., Narayanan V. K., Barris B. J., 2002, *MNRAS*, **330**, 443
- Blanton M. R., 2006, *ApJ*, **648**, 268
- Bogdán Á., Lovisari L., Volonteri M., Dubois Y., 2018, *ApJ*, **852**, 131
- Bois M., et al., 2011, *MNRAS*, **416**, 1654
- Bonfimi P., 2014, *PASP*, **126**, 935
- Bonfimi P., Zezas A., Birkinshaw M., Worrall D. M., Fabbiano G., O'Sullivan E., Trinchieri G., Wolter A., 2012, *MNRAS*, **421**, 2872
- Bonoli S., Mayer L., Callegari S., 2014, *MNRAS*, **437**, 1576
- Buchner J., 2024, [arXiv e-prints](https://arxiv.org/abs/2407.11127), p. [arXiv:2407.11127](https://arxiv.org/abs/2407.11127)
- Burstein D., Ho L. C., Huchra J. P., Macri L. M., 2005, *ApJ*, **621**, 246
- Busarello G., Longo G., Feoli A., 1992, *A&A*, **262**, 52
- Buta R. J., et al., 2015, *ApJS*, **217**, 32
- Campanelli M., Lousto C., Zlochower Y., Merritt D., 2007, *ApJ*, **659**, L5
- Caon N., Capaccioli M., D'Onofrio M., 1993, *MNRAS*, **265**, 1013
- Capaccioli M., Vietri M., 1988, in Fang L. Z., ed., Origin, Structure and Evolution of Galaxies. pp 150–161
- Capaccioli M., Caon N., Rampazzo R., 1990, *MNRAS*, **242**, 24P
- Capaccioli M., Vietri M., Held E. V., Lorenz H., 1991, *ApJ*, **371**, 535
- Cappellari M., et al., 2011, *MNRAS*, **416**, 1680
- Carter D., 1987, *ApJ*, **312**, 514
- Cellone S. A., Forte J. C., Geisler D., 1994, *ApJS*, **93**, 397
- Chen R., Peng B., Strom R. G., Wei J., 2011, *MNRAS*, **412**, 2433
- Chilingarian I. V., Mamon G. A., 2008, *MNRAS*, **385**, L83
- Chilingarian I., Cayatte V., Revaz Y., Dodonov S., Durand D., Durret F., Micol A., Slezak E., 2009, *Science*, **326**, 1379
- Ciambur B. C., 2015, *ApJ*, **810**, 120
- Ciambur B. C., 2016, *Publ. Astron. Soc. Australia*, **33**, e062
- Coccatto L., et al., 2009, *MNRAS*, **394**, 1249
- Conselice C. J., Gallagher John S. I., Wyse R. F. G., 2001, *AJ*, **122**, 2281
- D'Abrusco R., et al., 2013, *ApJ*, **773**, 87
- D'Abrusco R., Fabbiano G., Mineo S., Strader J., Fragos T., Kim D. W., Luo B., Zezas A., 2014, *ApJ*, **783**, 18
- D'Onghia E., Madau P., Vera-Ciro C., Quillen A., Hernquist L., 2016, *ApJ*, **823**, 4
- D'Onofrio M., Capaccioli M., Caon N., 1994, *MNRAS*, **271**, 523
- Daddi E., et al., 2005, *ApJ*, **626**, 680
- Damjanov I., et al., 2009, *ApJ*, **695**, 101
- Davis L. E., Cawson M., Davies R. L., Illingworth G., 1985, *AJ*, **90**, 169
- Davis B. L., Graham A. W., Cameron E., 2018, *ApJ*, **869**, 113
- Davis B. L., Graham A. W., Cameron E., 2019, *ApJ*, **873**, 85
- Davis T. A., et al., 2020, *MNRAS*, **496**, 4061
- De Bruyne V., Dejonghe H., Pizzella A., Bernardi M., Zeilinger W. W., 2001, *ApJ*, **546**, 903
- Doroshkevich A. G., Zel'dovich Y. B., Novikov I. D., 1967, *Soviet Ast.*, **11**, 233
- Douglas N. G., et al., 2007, *ApJ*, **664**, 257
- Draine B. T., Salpeter E. E., 1979, *ApJ*, **231**, 77
- Dreyer J. L. E., 1888, *Mem. RAS*, **49**, 1
- Dullo B. T., Graham A. W., 2012, *ApJ*, **755**, 163
- Dullo B. T., Graham A. W., 2014, *MNRAS*, **444**, 2700
- Dunn R. J. H., Allen S. W., Taylor G. B., Shurkin K. F., Gentile G., Fabian A. C., Reynolds C. S., 2010, *MNRAS*, **404**, 180
- Dwek E., 1998, *ApJ*, **501**, 643
- Eales S. A., et al., 2018, *MNRAS*, **481**, 1183
- Eggen O. J., Lynden-Bell D., Sandage A. R., 1962, *ApJ*, **136**, 748
- Emsellem E., et al., 2011, *MNRAS*, **414**, 888
- Erwin P., Beckman J. E., Pohlen M., 2005, *ApJ*, **626**, L81
- Event Horizon Telescope Collaboration et al., 2019, *ApJ*, **875**, L1
- Faber S. M., Jackson R. E., 1976, *ApJ*, **204**, 668
- Faber S. M., et al., 1997, *AJ*, **114**, 1771
- Fazio G. G., et al., 2004, *ApJS*, **154**, 10
- Ferrarese L., Merritt D., 2000, *ApJ*, **539**, L9
- Ferrarese L., et al., 2006, *ApJS*, **164**, 334
- Forbes D. A., Thomson R. C., 1992, *MNRAS*, **254**, 723
- Forbes D. A., Reitzel D. B., Williger G. M., 1995, *AJ*, **109**, 1576
- Forbes D. A., Brodie J. P., Huchra J., 1997, *AJ*, **113**, 887
- Forbes D. A., Sinpetru L., Savorgnan G., Romanowsky A. J., Usher C., Brodie J., 2017, *MNRAS*, **464**, 4611
- Franx M., Illingworth G. D., 1988, *ApJ*, **327**, L55
- Franx M., Illingworth G., Heckman T., 1989, *ApJ*, **344**, 613
- Fraser M., Casey A. R., Gilmore G., Heger A., Chan C., 2017, *MNRAS*, **468**, 418
- Gallagher John S. I., Ostriker J. P., 1972, *AJ*, **77**, 288
- Galliano F., et al., 2021, *A&A*, **649**, A18
- Gebhardt K., et al., 2000, *AJ*, **119**, 1157
- Genel S., et al., 2014, *MNRAS*, **445**, 175
- Goerdt T., Moore B., Read J. I., Stadel J., 2010, *ApJ*, **725**, 1707
- Gómez M., Richtler T., 2004, *A&A*, **415**, 499
- Gorbachev V. I., 1970, *Soviet Ast.*, **14**, 182
- Goudfrooij P., Norgaard-Nielsen H. U., Hansen L., Jorgensen H. E., de Jong T., 1990, *A&A*, **228**, L9
- Graham A. W., 2001, *MNRAS*, **326**, 543
- Graham A. W., 2002, *ApJ*, **568**, L13
- Graham A. W., 2004, *ApJ*, **613**, L33
- Graham A. W., 2012, *ApJ*, **746**, 113
- Graham A. W., 2013, in Oswalt T. D., Keel W. C., eds., , Vol. 6, Planets, Stars and Stellar Systems. Volume 6: Extragalactic Astronomy and Cosmology. Springer Science+Business Media, Dordrecht, pp 91–140, doi:10.1007/978-94-007-5609-0_2
- Graham A. W., 2014, in Seigar M. S., Treuhardt P., eds., Astronomical Society of the Pacific Conference Series Vol. 480, Structure and Dynamics of Disk Galaxies. p. 185 ([arXiv:1311.7207](https://arxiv.org/abs/1311.7207)), doi:10.48550/arXiv.1311.7207

- Graham A. W., 2019, *MNRAS*, **487**, 4995
- Graham A. W., 2020, *MNRAS*, **492**, 3263
- Graham A. W., 2023a, *MNRAS*, **518**, 6293
- Graham A. W., 2023b, *MNRAS*, **521**, 1023
- Graham A. W., 2023c, *MNRAS*, **522**, 3588
- Graham A. W., 2024, *MNRAS*
- Graham A. W., Driver S. P., 2005, *Publ. Astron. Soc. Australia*, **22**, 118
- Graham A. W., Driver S. P., 2007, *ApJ*, **655**, 77
- Graham A. W., Guzmán R., 2003, *AJ*, **125**, 2936
- Graham A. W., Sahu N., 2023a, *MNRAS*, **518**, 2177
- Graham A. W., Sahu N., 2023b, *MNRAS*, **520**, 1975
- Graham A. W., Sahu N., 2024, *MNRAS*, **530**, 3429
- Graham A. W., Scott N., 2013, *ApJ*, **764**, 151
- Graham A. W., Soria R., 2019, *MNRAS*, **484**, 794
- Graham A. W., Colless M. M., Busarello G., Zaggia S., Longo G., 1998, *A&AS*, **133**, 325
- Graham A. W., Erwin P., Caon N., Trujillo I., 2001, *ApJ*, **563**, L11
- Graham A. W., Erwin P., Trujillo I., Asensio Ramos A., 2003, *AJ*, **125**, 2951
- Graham A. W., Dullo B. T., Savorgnan G. A. D., 2015, *ApJ*, **804**, 32
- Graham A. W., Durré M., Savorgnan G. A. D., Medling A. M., Batcheldor D., Scott N., Watson B., Marconi A., 2016a, *ApJ*, **819**, 43
- Graham A. W., Ciambur B. C., Savorgnan G. A. D., 2016b, *ApJ*, **831**, 132
- Graham A. W., Janz J., Penny S. J., Chilingarian I. V., Ciambur B. C., Forbes D. A., Davies R. L., 2017, *ApJ*, **840**, 68
- Graham A. W., Soria R., Ciambur B. C., Davis B. L., Swartz D. A., 2021, *ApJ*, **923**, 146
- Graham A. W., Jarrett T. H., Cluver M. E., 2024, *MNRAS*, **527**, 10059
- Gualandris A., Merritt D., 2008, *ApJ*, **678**, 780
- Gualandris A., Merritt D., 2012, *ApJ*, **744**, 74
- Gunn J. E., Gott J. Richard I., 1972, *ApJ*, **176**, 1
- Guo Q., et al., 2011, *MNRAS*, **413**, 101
- Hansen L., Norgaard-Nielsen H. U., Jorgensen H. E., 1985, *A&A*, **149**, 442
- Hawking S. W., 1975, *Communications in Mathematical Physics*, **43**, 199
- Heckman T. M., Illingworth G. D., Miley G. K., van Breugel W. J. M., 1985, *ApJ*, **299**, 41
- Hernquist L., Quinn P. J., 1988, *ApJ*, **331**, 682
- Herschel J. F. W., 1864, *Philosophical Transactions of the Royal Society of London Series I*, **154**, 1
- Hickson P., 1982, *ApJ*, **255**, 382
- Hon D. S. H., Graham A. W., Davis B. L., Marconi A., 2022, *MNRAS*, **514**, 3410
- Hon D. S. H., Graham A. W., Sahu N., 2023, *MNRAS*, **519**, 4651
- Hubble E. P., 1926, *ApJ*, **64**, 321
- Hubble E. P., 1936, *Realm of the Nebulae*. New Haven: Yale University Press
- Ideta M., Makino J., 2004, *ApJ*, **616**, L107
- Jaffe W., Ford H. C., O'Connell R. W., van den Bosch F. C., Ferrarese L., 1994, *AJ*, **108**, 1567
- Jeans J. H., 1919, *Problems of cosmogony and stellar dynamics*. Cambridge Univ. Press, Cambridge
- Jeans J. H., 1928, *Astronomy and cosmogony*. Cambridge: Cambridge University Press
- Jedrzejewski R. I., 1987, *MNRAS*, **226**, 747
- Jedrzejewski R., Schechter P. L., 1989, *AJ*, **98**, 147
- Jog C. J., Maybhate A., 2006, *MNRAS*, **370**, 891
- Johnston E. J., Hau G. K. T., Coccato L., Herrera C., 2018, *MNRAS*, **480**, 3215
- Kant I., 1755, *Allgemeine Naturgeschichte und Theorie des Himmels* (in German). Universal Natural History and Theory of the Heavens (p.367). Königsberg, Germany. Translated by Stephen Palmquist in Kant's Critical Religion (in 2000). Ashgate, Aldershot, p.320
- Karachentsev I. D., Kroupa P., 2024, *MNRAS*, **528**, 2805
- Karachentsev I. D., Nasonova O. G., Karachentseva V. E., 2015, *Astrophysical Bulletin*, **70**, 1
- Kaviraj S., et al., 2012, *MNRAS*, **423**, 49
- Khan F. M., Holley-Bockelmann K., Berczik P., Just A., 2013, *ApJ*, **773**, 100
- Khandai N., Feng Y., DeGraf C., Di Matteo T., Croft R. A. C., 2012, *MNRAS*, **423**, 2397
- Koch A., Burkert A., Rich R. M., Collins M. L. M., Black C. S., Hilker M., Benson A. J., 2012, *ApJ*, **755**, L13
- Kormendy J., Richstone D., 1995, *ARA&A*, **33**, 581
- Krajnović D., et al., 2011, *MNRAS*, **414**, 2923
- Krajnović D., et al., 2013, *MNRAS*, **432**, 1768
- Kulkarni G., Loeb A., 2012, *MNRAS*, **422**, 1306
- LaMassa S. M., Heckman T. M., Ptak A., Urry C. M., 2013, *ApJ*, **765**, L33
- Labbe I., et al., 2023, *arXiv e-prints*, p. arXiv:2306.07320
- Lahén N., Johansson P. H., Rantala A., Naab T., Frigo M., 2018, *MNRAS*, **475**, 3934
- Laor A., 2001, *ApJ*, **553**, 677
- Laplace P. S., 1796, *Exposition du Système du monde*. Cercie-Social, Paris. Exposition of the System of the World, translated from French by J. Pond (London: R. Philips, 1809)
- Läsker R., Ferrarese L., van de Ven G., 2014, *ApJ*, **780**, 69
- Laurikainen E., Salo H., Buta R., 2005, *MNRAS*, **362**, 1319
- Li Y., et al., 2020, *ApJ*, **895**, 102
- Liller M. H., 1966, *ApJ*, **146**, 28
- Lima Neto G. B., Gerbal D., Márquez I., 1999, *MNRAS*, **309**, 481
- Liu B., Bromm V., 2022, *ApJ*, **937**, L30
- Loubser S. I., Lagos P., Babul A., O'Sullivan E., Jung S. L., Olivares V., Kolokythas K., 2022, *MNRAS*, **515**, 1104
- Magorrian J., et al., 1998, *AJ*, **115**, 2285
- Maiolino R., et al., 2024, *Nature*, **627**, 59
- Malin D. F., 1985, in Nieto J. L., ed., , Vol. 232, *New Aspects of Galaxy Photometry*. Springer-Verlag Berlin, Heidelberg New York, p. 27, doi:10.1007/BFb0030917
- Malin D. F., Carter D., 1983, *ApJ*, **274**, 534
- Marinoni C., Monaco P., Giuricin G., Costantini B., 1999, *ApJ*, **521**, 50
- Matthias M., Gerhard O., 1999, *MNRAS*, **310**, 879
- Merritt D., Mikkola S., Szell A., 2007, *ApJ*, **671**, 53
- Michard R., 1984, *A&A*, **140**, L39
- Michard R., Simien F., 1988, *A&AS*, **74**, 25
- Michell J., 1784, *Philosophical Transactions of the Royal Society of London Series I*, **74**, 35
- Milosavljević M., Merritt D., 2001, *ApJ*, **563**, 34
- Muñoz-Mateos J. C., et al., 2015, *ApJS*, **219**, 3
- Mulchaey J. S., Davis D. S., Mushotzky R. F., Burstein D., 2003, *ApJS*, **145**, 39
- Nieto J. L., Coupinot G., Lelievre G., Madsen C., 1983, *MNRAS*, **203**, 39P
- Nieto J. L., Capaccioli M., Held E. V., 1988, *A&A*, **195**, L1
- Nieto J. L., Poulain P., Davoust E., 1994, *A&A*, **283**, 1
- Nowak N., Thomas J., Erwin P., Saglia R. P., Bender R., Davies R. I., 2010, *MNRAS*, **403**, 646
- Nykytyuk T., 2015, *Advances in Space Research*, **55**, 2372
- Paudel S., et al., 2023, *MNRAS*, **526**, L136
- Pawlowski M. S., Kroupa P., 2020, *MNRAS*, **491**, 3042
- Pellegrini S., Held E. V., Ciotti L., 1997, *MNRAS*, **288**, 1
- Peng C. Y., Ho L. C., Impey C. D., Rix H.-W., 2002, *AJ*, **124**, 266
- Perley R. A., Bridle A. H., Willis A. G., 1984, *ApJS*, **54**, 291
- Pfeffer J., Baumgardt H., 2013, *MNRAS*, **433**, 1997
- Pierini D., Zibetti S., Braglia F., Böhringer H., Finoguenov A., Lynam P. D., Zhang Y. Y., 2008, *A&A*, **483**, 727
- Pietrzyński G., et al., 2019, *Nature*, **567**, 200
- Pinkney J., et al., 2003, *ApJ*, **596**, 903
- Planck Collaboration et al., 2020, *A&A*, **641**, A6
- Pohlen M., Dettmar R. J., Lütticke R., Aronica G., 2002, *A&A*, **392**, 807
- Price J., et al., 2009, *MNRAS*, **397**, 1816
- Prichard L. J., Vaughan S. P., Davies R. L., 2019, *MNRAS*, **488**, 1679
- Prieur J. L., 1988, *ApJ*, **326**, 596
- Quinn P. J., Hernquist L., Fullagar D. P., 1993, *ApJ*, **403**, 74
- Raimundo S. I., 2021, *A&A*, **650**, A34
- Rest A., van den Bosch F. C., Jaffe W., Tran H., Tsvetanov Z., Ford H. C., Davies J., Schafer J., 2001, *AJ*, **121**, 2431
- Reynolds J. H., 1925, *MNRAS*, **85**, 1014
- Rhode K. L., Zepf S. E., 2004, *AJ*, **127**, 302

- Richings A. J., Uttley P., K rding E., 2011, *MNRAS*, **415**, 2158
- Richstone D. O., Tremaine S., 1988, *ApJ*, **327**, 82
- Rickes M. G., Pastoriza M. G., Bonatto C., 2009a, *A&A*, **505**, 73
- Rickes M. G., Pastoriza M. G., Bonatto C., 2009b, *A&A*, **505**, 73
- Rix H.-W., Franx M., Fisher D., Illingworth G., 1992, *ApJ*, **400**, L5
- Romanowsky A. J., Douglas N. G., Arnaboldi M., Kuijken K., Merrifield M. R., Napolitano N. R., Capaccioli M., Freeman K. C., 2003, *Science*, **301**, 1696
- Roos N., Norman C. A., 1979, *A&A*, **76**, 75
- Rosado P. A., Sesana A., Gair J., 2015, *MNRAS*, **451**, 2417
- Rusli S. P., Erwin P., Saglia R. P., Thomas J., Fabricius M., Bender R., Nowak N., 2013, *AJ*, **146**, 160
- Rutherford T. H., et al., 2024, *MNRAS*,
- S4G team 2015, Spitzer Survey of Stellar Structure in Galaxies, doi:10.26131/IRSA425, <https://irsa.ipac.caltech.edu/data/SPITZER/S4G>
- Sahu N., Graham A. W., Davis B. L., 2019a, *ApJ*, **876**, 155
- Sahu N., Graham A. W., Davis B. L., 2019b, *ApJ*, **887**, 10
- Sambhus N., Gerhard O., M ndez R. H., 2006, *AJ*, **131**, 837
- Sandage A., Binggeli B., Tammann G. A., 1985, *AJ*, **90**, 1759
- Savorgnan G. A. D., Graham A. W., 2016, *ApJS*, **222**, 10
- Schauer A. T. P., Remus R.-S., Burkert A., Johansson P. H., 2014, *ApJ*, **783**, L32
- Schawinski K., et al., 2014, *MNRAS*, **440**, 889
- Schlafly E. F., Finkbeiner D. P., 2011, *ApJ*, **737**, 103
- Schlegel D. J., Finkbeiner D. P., Davis M., 1998, *ApJ*, **500**, 525
- Schwarzschild M., Spitzer L., 1953, *The Observatory*, **73**, 77
- Scorza C., Bender R., 1995a, *A&A*, **293**, 20
- Scorza C., Bender R., 1995b, *A&A*, **293**, 20
- Scorza C., van den Bosch F. C., 1998, *MNRAS*, **300**, 469
- Scott N., Graham A. W., Schombert J., 2013, *ApJ*, **768**, 76
- Seigar M. S., Graham A. W., Jerjen H., 2007, *MNRAS*, **378**, 1575
- S rsic J. L., 1963, *Bolet n de la Asociaci n Argentina de Astronom a La Plata Argentina*, **6**, 41
- Sersic J. L., 1968, *Atlas de Galaxias Australes*. Observatorio Astronomico, Cordoba, Argentina
- Shapiro S. L., Teukolsky S. A., 1985, *ApJ*, **292**, L41
- Sheth K., et al., 2010, *PASP*, **122**, 1397
- Singh J., Monaco P., Tan J. C., 2023, *MNRAS*, **525**, 969
- Spiniello C., Napolitano N. R., Coccato L., Pota V., Romanowsky A. J., Tortora C., Covone G., Capaccioli M., 2015, *MNRAS*, **452**, 99
- Spitzer L. J., Baade W., 1951, *ApJ*, **113**, 413
- Spolyar D., Bodenheimer P., Freese K., Gondolo P., 2009, *ApJ*, **705**, 1031
- Statler T. S., Smecker-Hane T., 1999, *AJ*, **117**, 839
- Swedenborg E., 1734, *Principia rerum naturalium sive novorum tantaminium phenomena mundi elementaris philosophice explicandi*. Friedrich Hekel, Dresden and Leipzig
- Teodorescu A. M., M ndez R. H., Bernardi F., Riffeser A., Kudritzki R. P., 2010, *ApJ*, **721**, 369
- Theureau G., Hanski M. O., Coudreau N., Hallet N., Martin J. M., 2007, *A&A*, **465**, 71
- Tisserand P., et al., 2007, *A&A*, **469**, 387
- Tonry J. L., Dressler A., Blakeslee J. P., Ajhar E. A., Fletcher A. B., Luppino G. A., Metzger M. R., Moore C. B., 2001, *ApJ*, **546**, 681
- Toomre A., 1977, in Tinsley B. M., Larson Richard B., Gehret D. C., eds, *Evolution of Galaxies and Stellar Populations*. p. 401
- Torres-Orjuela A., Huang S.-J., Liang Z.-C., Liu S., Wang H.-T., Ye C.-Q., Hu Y.-M., Mei J., 2023, *arXiv e-prints*, p. arXiv:2307.16628
- Tremaine S. D., Ostriker J. P., Spitzer L. J., 1975, *ApJ*, **196**, 407
- Trujillo I., Erwin P., Asensio Ramos A., Graham A. W., 2004, *AJ*, **127**, 1917
- Trujillo I., Ferr -Mateu A., Balcells M., Vazdekis A., S nchez-Bl zquez P., 2014, *ApJ*, **780**, L20
- Umeda H., Nomoto K., 2003, *Nature*, **422**, 871
- Umemura M., Loeb A., Turner E. L., 1993, *ApJ*, **419**, 459
- Vasiliev E., Antonini F., Merritt D., 2015, *ApJ*, **810**, 49
- Villanueva-Domingo P., Mena O., Palomares-Ruiz S., 2021, *Frontiers in Astronomy and Space Sciences*, **8**, 87
- Vogelsberger M., et al., 2014, *MNRAS*, **444**, 1518
- Vorontsov-Velyaminov B. A., 1959, *Atlas and Catalog of Interacting Galaxies* (1959, p. 0
- Waggett P. C., Warner P. J., Baldwin J. E., 1977, *MNRAS*, **181**, 465
- Wagner S. J., Bender R., Moellenhoff C., 1988, *A&A*, **195**, L5
- Wandel A., 1999, *ApJ*, **519**, L39
- Werner P. N., Worrall D. M., Birkinshaw M., 2000, *MNRAS*, **317**, 105
- Werner M. W., et al., 2004, *ApJS*, **154**, 1
- Whitmore B. C., Lucas R. A., McElroy D. B., Steiman-Cameron T. Y., Sackett P. D., Olling R. P., 1990, *AJ*, **100**, 1489
- Willmer C. N. A., 2018, *ApJS*, **236**, 47
- Wu X., Roby T., Ly L., 2010, in Mizumoto Y., Morita K. I., Ohishi M., eds, *Astronomical Society of the Pacific Conference Series Vol. 434*, *Astronomical Data Analysis Software and Systems XIX*. p. 14
- Xu H.-G., Gu J.-H., Gu L.-Y., Zhang Z.-L., Wang Y., An T., 2010, *Research in Astronomy and Astrophysics*, **10**, 220
- Yoon Y., Lim G., 2020, *ApJ*, **905**, 154
- Yoon S.-J., Sohn S. T., Kim H.-S., Chung C., Cho J., Lee S.-Y., Blakeslee J. P., 2013, *ApJ*, **768**, 137
- Young C. K., Currie M. J., 1994, *MNRAS*, **268**, L11
- Yuan G.-W., et al., 2023, *arXiv e-prints*, p. arXiv:2303.09391
- Zel'dovich Y. B., Podurets M. A., 1965, *Azh*, **42**, 963
- Zepf S. E., Ashman K. M., Geisler D., 1995, *ApJ*, **443**, 570
- Zezas A., Hernquist L., Fabbiano G., Miller J., 2003, *ApJ*, **599**, L73
- Ziparo F., Gallerani S., Ferrara A., Vito F., 2022, *MNRAS*, **517**, 1086
- Ziparo F., Ferrara A., Sommovigo L., Kohandel M., 2023, *MNRAS*, **520**, 2445
- de Lorenzi F., Gerhard O., Saglia R. P., Sambhus N., Debatista V. P., Pannella M., M ndez R. H., 2008, *MNRAS*, **385**, 1729
- de Vaucouleurs' G., 1953, *MNRAS*, **113**, 134
- de Vaucouleurs G., Capaccioli M., 1979, *ApJS*, **40**, 699
- de Vaucouleurs G. H., de Vaucouleurs A., Shapley H., 1964, *Reference catalogue of bright galaxies*. University of Texas Press, Austin
- de Vaucouleurs G., de Vaucouleurs A., Corwin Herold G. J., Buta R. J., Paturel G., Fouque P., 1991, *Third Reference Catalogue of Bright Galaxies*. Springer, New York
- van Dokkum P. G., Franx M., 1995, *AJ*, **110**, 2027
- van den Bergh S., 1976, *ApJ*, **206**, 883
- van den Bergh S., 1990, *ApJ*, **348**, 57
- van den Bosch F. C., Jaffe W., van der Marel R. P., 1998, *MNRAS*, **293**, 343

APPENDIX A: UNCOVERING HIDDEN DISCS

A1 A trio of lenticular galaxies (S0)

A1.1 NGC 4649 (M60)

NGC 4649 was not modelled to sufficiently large radii in Sahu et al. (2019a) to clearly detect the large-scale disc-like component whose kinematics were observed by Arnold et al. (2014) to extend to at least four arcminutes. Comparing with the simulations of Bois et al. (2011), Bellstedt et al. (2017a) note that NGC 4649 is consistent with being an E galaxy that is a fast-rotating merger remnant. The system's net angular momentum has not been cancelled in the merger, and a (hot disc-like) structure with significant rotation remains. The passage of (old or young) satellites through discs can also heat them (D'Onghia et al. 2016). Remodelling the light profile of NGC 4649 to six arcminutes (Fig. A1) yields a galaxy (model-extrapolated) 3.6 μm magnitude of 8.16 mag and a S rsic spheroid magnitude of 8.85 mag when including a single large-scale exponential disc. This yields a B/T ratio of 0.53. From an initial luminosity distance of 16.2 ± 1.1 Mpc (Tonry et al. 2001), and after a 0.083 mag correction/reduction to the distance modulus (Blakeslee et al. 2002; Pietrzyński et al. 2019), and with $(B - V)_{\text{vega}} = 0.95$ and thus $M_*/L_{3.6} = 0.82$ (Graham & Sahu 2023a, their equation 4), the logarithm of the galaxy stellar mass is 11.48 dex. This is just 0.08

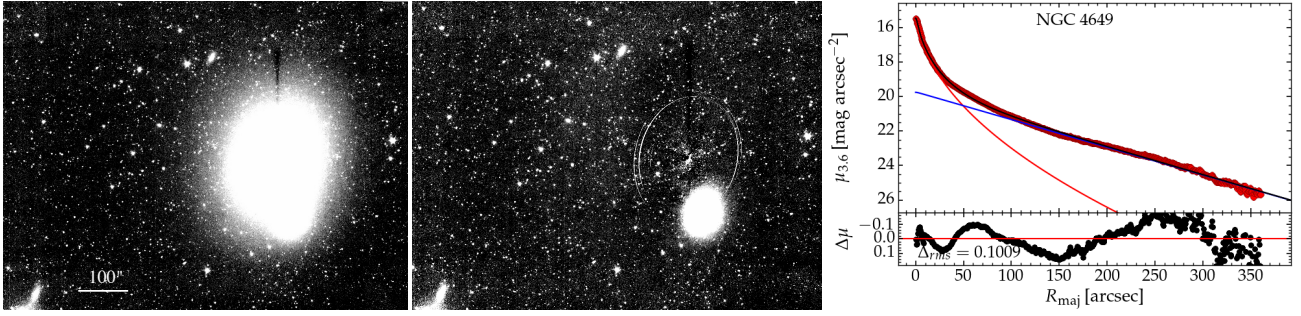


Figure A1. Left: Similar to Fig. 1 but for NGC 4649 (M60), which has a remarkably similar light distribution. Image courtesy of *SHA*. The scale bar is $100'' = 7.8$ kpc long. Middle: Residual image after removing the symmetrical light distribution in NGC 4649, thereby better revealing NGC 4647. Right: Major axis light profile decomposed into a Sérsic spheroid (red curve: $R_{e,\text{maj}} = 22''.5$, $\mu_e = 18.61$ mag arcsec $^{-2}$, and $n_{\text{maj}} = 2.04$) and exponential disc (straight blue line: $\mu_0 = 19.73$ mag arcsec $^{-2}$, $h_{\text{disc,maj}} = 68'' = 5.3$ kpc). The disc is also evident in the kinematic map from [Krajnović et al. \(2011, their figure C1\)](#).

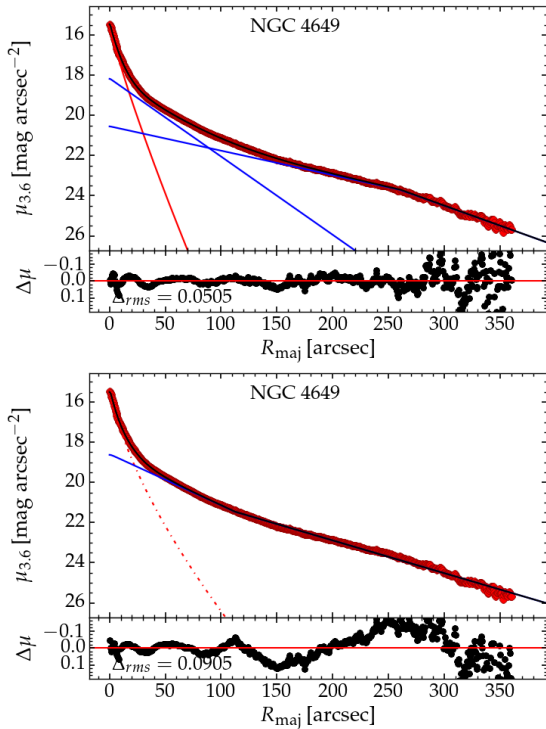


Figure A2. Similar to Fig. 2 but for NGC 4649. Top panel: Sérsic spheroid (red curve: $R_{e,\text{maj}} = 9''.84$ and $n_{\text{maj}} = 1.33$) plus intermediate-scale disc (straight blue line: $\mu_0 = 18.20$ mag arcsec $^{-2}$, $h = 28''.4 = 2.2$ kpc) and weakly-truncated (at $r = 260''$) large-scale disc (bent blue line: $\mu_0 = 20.58$ mag arcsec $^{-2}$, $h_{\text{inner}} = 90'' = 7$ kpc, $h_{\text{outer}} = 55'' = 4.3$ kpc). Bottom panel: Spheroid (red curve: $R_{e,\text{maj}} = 12''.7$, $n_{\text{maj}} = 1.46$, and $\mu_e = 17.84$ mag arcsec $^{-2}$) plus anti-truncated disc (bent blue line: $\mu_0 = 18.58$ mag arcsec $^{-2}$, $R_{\text{bend}} = 113''$, $h_{\text{inner}} = 42''.4 = 3.3$ kpc, $h_{\text{outer}} = 66''.6 = 5.2$ kpc). Note: as seen in the upper panel, an additional downward bend at $r \approx 260''$ would improve the fit in the lower panel.

ever, the spheroid mass may still be too high for the same reasons²² as seen with NGC 3379 in Section 2.3.1.

As with NGC 3379 (Section 2.3.1), adding a second (intermediate-scale) disc to NGC 4649 does not affect the total galaxy magnitude derived from the spheroid plus single exponential disc fit above but improves the fit. The residual light profile in the top panel of Fig. A2 is notably improved compared to that in Fig. A1. The spheroid magnitude changes from 8.85 to 9.82 mag, which is ~ 1 mag fainter than acquired when fitting a Sérsic plus (single) large-scale exponential component. The new B/T flux ratio in NGC 4649 is 0.22. The lower panel of Fig. A2 reveals how an anti-truncated disc effectively captures the inner, intermediate-scale disc and the outer large-scale disc. The hump in the residual light profile from ~ 150 to ~ 350 arcseconds, previously seen in Fig. A1, can be removed with the introduction of a second bend in the new disc model, matching the single bend at $\sim 260''$ in the truncated exponential disc model used in the upper panel of Fig. A2. However, as with the light profile for NGC 3379, this second bend at $r \sim 260''$ commences at $\mu_{3,6} \approx 24$ mag arcsec $^{-2}$ and could result from an over-subtraction of the ‘sky background’ for this galaxy, the third brightest in the Virgo Cluster, or perhaps due to contamination from NGC 4647. Finally, as with the discussion around NGC 3379, the need for a large partially depleted core in NGC 4649 ([Ferrarese et al. 2006](#); [Dullo & Graham 2014](#)) is diminished after adding disc component(s) that reduce the bulge Sérsic index from > 2 to < 2 . This is evident from the inner-most region of the residual light profiles in Fig. A1 and Fig. A2

A1.2 NGC 4697

A *Spitzer/IRAC1* $3.6 \mu\text{m}$ image of NGC 4697 was taken from S⁴G. Again, a basic but inadequate Sérsic-bulge + exponential-disc model was created (Fig. A3). The snake-like residual light profile suggests there is more going on. The first bump in the ellipticity

²² A dimmed galaxy magnitude is a common occurrence when adding a large-scale disc because the extrapolated model’s light at large radii coming from an extrapolated exponential, i.e., a Sérsic $n = 1$, disc model is generally less than that from an extrapolated single-Sérsic galaxy model with $n > 1$. This is one of the reasons why vast numbers of automated single-Sérsic fits to massive galaxies overestimate their luminosities. Of course, while the two-component fit gives improved/stable galaxy magnitudes, the component parameters can still be quite erroneous, as repeatedly illustrated here in Section A1.1.

dex less than previously obtained ([Graham & Sahu 2023a](#)). How-



Figure A3. Similar to Fig. 1 but for NGC 4697. *Spitzer/IRAC1* 3.6 μm image courtesy of S⁴G (pipeline 1 image: Muñoz-Mateos et al. 2015). The scale bar is 150'' = 8.1 kpc long. Right panel: The open circles were excluded from the fit. For reference: $n_{\text{sph,maj}} = 2.4$, $R_{\text{e,sph,maj}} = 24''$, $\mu_{\text{e,sph}} = 18.98 \text{ mag arcsec}^{-2}$, $\mu_{0,\text{disc}} = 20.22 \text{ mag arcsec}^{-2}$, and $h_{\text{disc,maj}} = 68''$.

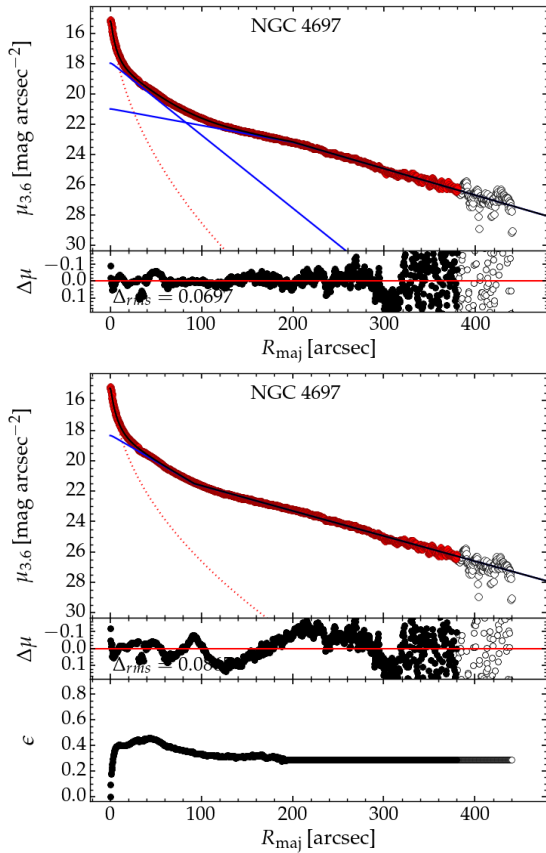


Figure A4. Similar to Fig. 2 but for NGC 4697. Lower panel: Major axis light profile fit with a Sérsic spheroid (red curve, $R_{\text{e,maj}} = 9''.5$ and $n_{\text{maj}} = 2.12$) and an anti-truncated disc (bent blue line, $\mu_0 = 18.27$, $R_{\text{bend,maj}} = 92''$, $h_{\text{inner,maj}} = 31'' = 1.67 \text{ kpc}$, and $h_{\text{outer,maj}} = 65'' = 3.51 \text{ kpc}$). This ‘hot’ outer disc model gives a bulge (aka spheroid) magnitude of 10.39 mag and a total galaxy magnitude of 8.74 mag, as mentioned in Section A1.2.

profile peaks at 9'' (Savorgnan & Graham 2016), and Läscher et al. (2014) reported two embedded discs in this galaxy. Krajnović et al. (2011, their figure C1) report rotation of $\pm 131 \text{ km s}^{-1}$ over the inner 30'', which had been shown to extend to $\sim 90''$ (de Lorenzi et al. 2008) along the major axis. From the final analysis (preferred fit) performed here (Fig. A4), the total galaxy magnitude at 3.6 μm is 8.74 mag. Breaking from the traditional interpretation that NGC 4697 is an E galaxy, it is an ES or S0 galaxy. Graham & Sahu (2023b) regarded it as an ES galaxy, but if the outer structure

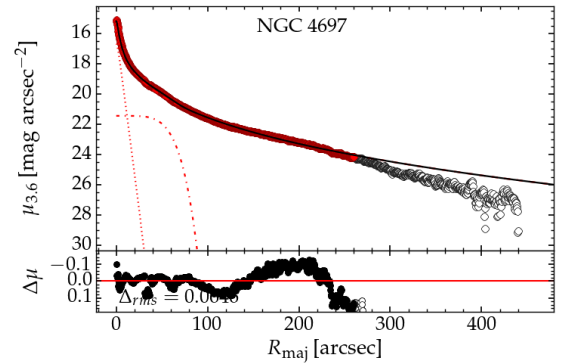


Figure A5. Sub-optimal (and rejected) fit to the major axis of NGC 4697. The dominant Sérsic spheroid (red curve) has $R_{\text{e,maj}} = 80''$, $n_{\text{maj}} = 3.6$, and contains 91.5 per cent of the total extrapolated flux. Attempts to fit such a dominant Sérsic spheroid with embedded discs (Savorgnan & Graham 2016) results in an overestimation of the light at large radii.

is rotating sufficiently fast, it may be considered an S0 galaxy. As with NGC 4278 and NGC 4494 (previously mentioned but not in the current sample), Bellstedt et al. (2017a) report an upturn in the spin parameter for NGC 4697 beyond $\sim 100''$, which is roughly the galaxy’s major axis half-light radius (Forbes et al. 2017). In addition to a thin, intermediate-scale disc, captured by the inner, steeper part of the anti-truncated disc model in Fig. A4, NGC 4697 is modelled with a thick (‘hot’) large-scale disc, captured by the outer part of this anti-truncated disc model. This double disc structure is supported by the kinematics maps of Arnold et al. (2014, see their figure 14), where the data extends to $146''$ along the major axis, and the inner disc extends to $100 \pm 20''$. Fitting an anti-truncated disc model to capture the two discs gives a spheroid magnitude of 10.39 mag and a B/T ratio of 0.22. At a luminosity distance of $11.3 \pm 0.7 \text{ Mpc}$ (Tonry et al. 2001; Blakeslee et al. 2002; Pietrzyński et al. 2019), and using $M/L = 0.70$ (Graham & Sahu 2023a), the logarithm of the spheroid’s stellar mass is 10.20 dex.

If a disc becomes too ‘hot’, it will resemble a spheroid, and this may be what we are witnessing in NGC 4697, where the outer component visually resembles a spheroid but rotates more like a disc. Carter (1987) characterised NGC 4697 as a rapidly rotating E galaxy with an embedded weak disc. Läscher et al. (2014) labelled the weak disc as embedded within an ‘envelope’ instead of a spheroid. Although NGC 4697 is only a BCG, it appears to be an S0 galaxy (Fig. A4) rather than an ES galaxy (Fig. A5), as modelled in Savorgnan & Graham (2016). From the kinematic maps of Arnold

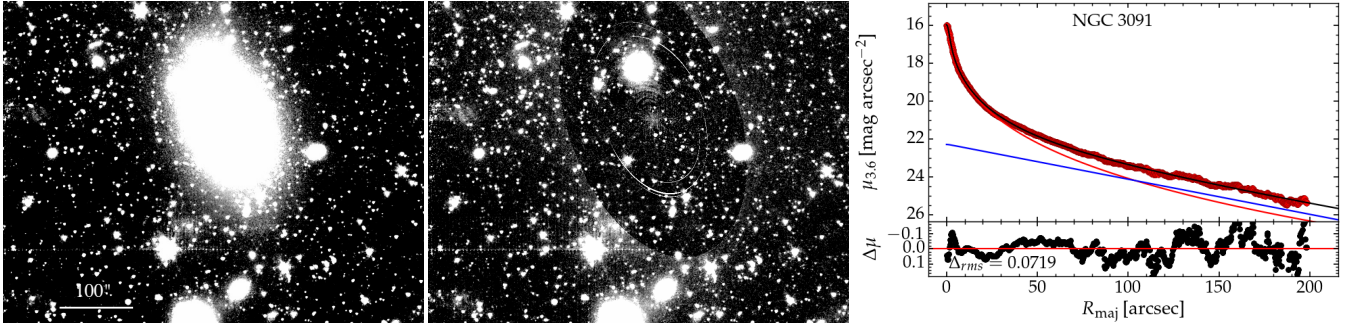


Figure A6. Similar to Fig. 1 but for NGC 3091. Image courtesy of *SHA*. The scale bar is $100'' = 27.6$ kpc long. Sérsic bulge (red curve: $\mathfrak{M}_{3.6} = 10.73$ mag, $n_{\text{maj}} = 3.47$, $R_{e,\text{maj}} = 24''.1$) plus exponential disc (straight blue line: $\mathfrak{M}_{3.6} = 11.88$ mag, $h_{\text{maj}} = 59''.3$).

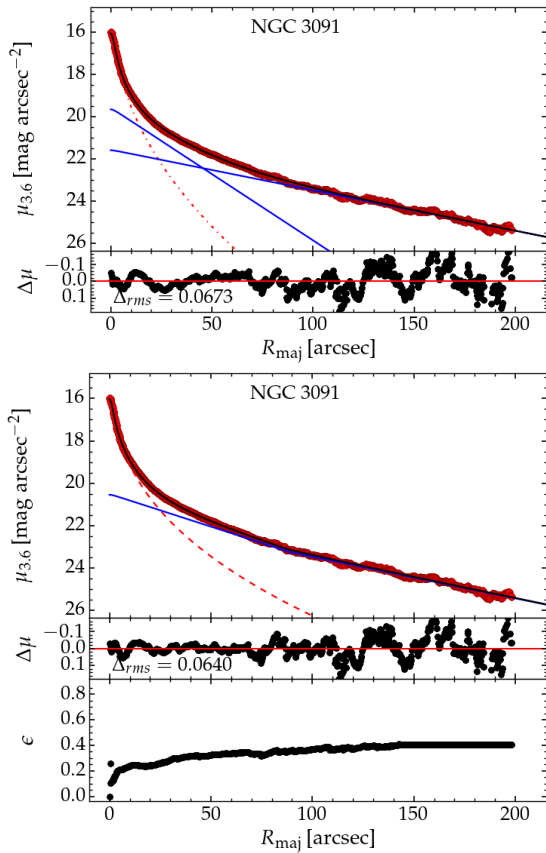


Figure A7. Alternative (preferred) fits for NGC 3091. Upper panel: An intermediate-scale disc ($\mu_0 = 19.57$ mag arcsec $^{-2}$, $h = 17''.3 = 4.8$ kpc) and large-scale disc ($\mu_0 = 21.56$ mag arcsec $^{-2}$, $h = 57'' = 15.7$ kpc), plus a Sérsic bulge (red curve: $\mu_e = 18.75$ mag arcsec $^{-2}$, $n_{\text{maj}} = 2.17$, and $R_{e,\text{maj}} = 7''.0$). Lower panel: Sérsic spheroid (red curve: $R_{e,\text{maj}} = 11''.4$, $\mu_e = 19.43$ mag arcsec $^{-2}$, and $n_{\text{maj}} = 2.67$) plus anti-truncated disc (bent blue line: $\mu_0 = 20.51$ mag arcsec $^{-2}$, $h_{\text{inner,maj}} = 35'' = 9.7$ kpc, $R_{\text{bend,maj}} = 88''$, $h_{\text{outer,maj}} = 55'' = 15.2$ kpc). The disc magnitude is 11.12 mag, and the total galaxy magnitude is 10.42 mag.

et al. (2014, see their figure 14), the V/σ ratio beyond the inner disc may be around 1, reflective of a heated disc (with $\sigma > 50$ km s^{-1} that is transitioning to a spheroid). To err on the side of caution, this galaxy is grouped with the S0 galaxies and thus excluded from the E/ES sample. NGC 821 and NGC 3377 appear as more evolved versions of NGC 4697, such that their outer component (hot disc

now spheroid) do not have quite the same level of ‘spin’ (Bellstedt et al. 2017a, their figure 11).

A1.3 NGC 3091

NGC 3091 was shown to rotate fast by Franx et al. (1989), reaching a rotational speed of 96 km s^{-1} by $14''$, as confirmed by Busarello et al. (1992). Furthermore, its ellipticity profile asymptotes to 0.4 at $R_{\text{maj}} = 200''$, suggesting a large-scale disc rather than (solely) an intermediate-scale disc is present. Moreover, upon closer inspection, E4 galaxies are almost always found to be S0 galaxies. The light profile from NGC 3091 is fit with a Sérsic-bulge plus an exponential-disc in Fig. A6. The total $3.6 \mu\text{m}$ galaxy magnitude is 10.41 mag. However, once again, a better fit for NGC 3091 contains an anti-truncated disc (Fig. A7), giving a revised total magnitude of 10.42 mag. In passing, it is noted that the 15 kpc scale-length of the outer half of the disc is large and may be indicative that something else is afoot. Possibly, there is some contribution of halo/envelope, as NGC 3091 resides in a compact group of galaxies (Hickson 1982) where encounters may strip stars from galaxies and start to build the intragroup light. Curiously, Seigar et al. (2007) discovered a tendency for the envelopes of BCGs to be exponential, a result subsequently seen by Pierini et al. (2008). Furthermore, the cores in some of these galaxies, built from infalling dense galaxy nuclei (Goerdt et al. 2010) rather than just massive black holes, may be great enough that the central spheroid takes on a low Sérsic index in a process dubbed ‘galforming’ (Graham & Sahu 2023b). Also worth bearing in mind are the planes-of-satellites around massive S galaxies (e.g. Pawlowski & Kroupa 2020; Karachentsev & Kroupa 2024, and references therein) that are, arguably, related to pre-merger encounters (Banik et al. 2022).

Using a Galactic-extinction-corrected $(B - V)_{\text{Vega}}$ colour of 0.96 mag gives $M_*/L_{3.6} = 0.84$ (Graham & Sahu 2023a, their equation 4). At a luminosity distance of 58.6 ± 10.9 Mpc (Theureau et al. 2007), the galaxy’s $3.6 \mu\text{m}$ absolute magnitude $\mathfrak{M}_{3.6} = -23.43$ mag, and, as before, using $\mathfrak{M}_{\odot,3.6} = 6.02$ (AB mag: Willmer 2018), the logarithm of the galaxy stellar mass is 11.70 dex, 0.16 dex less than reported in (Graham & Sahu 2023a) based on a single Sérsic fit. Having a ‘fast rotating’ ETG with such a high stellar mass is unusual. The logarithm of the spheroid mass is roughly half this value, at 11.38 dex when using the anti-truncated disc model, and it drops to 11.25 dex when additionally including a nuclear component. The residual and ellipticity profile suggests a nuclear ($\sim 2''$) disc-like component may exist. Fitting for this changed the anti-truncated disc magnitude to 10.98 mag and dimmed the bulge magnitude to 11.55 mag ($n_{\text{maj}} = 2.36 \pm 0.14$, and $R_{e,\text{maj}} = 11''.4 \pm 0.72$).

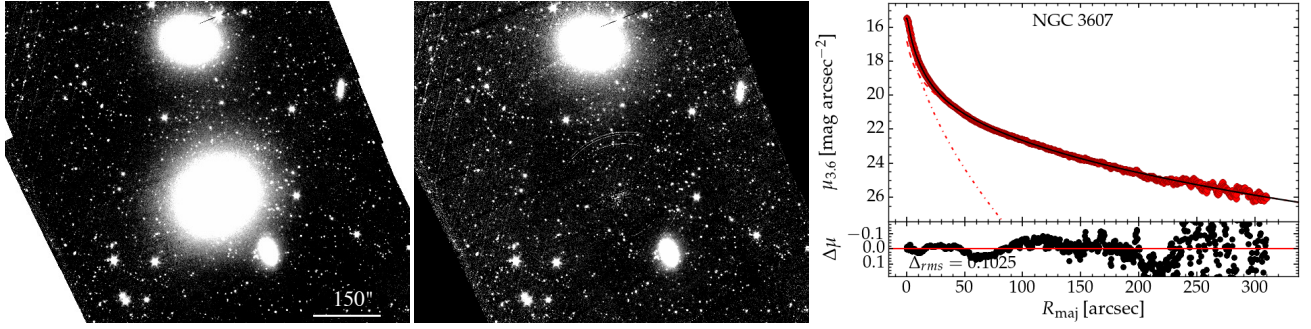


Figure A8. Similar to Fig. 1 but for NGC 3607. Image courtesy of S⁴G. The scale bar is 150'' = 18.0 kpc long. A Sérsic model has been used for the large-scale spheroidal component ($n_{\text{maj}} = 3.06$, $R_{e,\text{maj}} = 59''.8$, and $\mu_e = 21.52 \text{ mag arcsec}^{-2}$) and also for the inner disc component(s): $n_{\text{maj}} = 1.80$, $R_{e,\text{maj}} = 8''.4 = 1.0 \text{ kpc}$, $\mu_e = 18.29 \text{ mag arcsec}^{-2}$. NGC 3605 is in the lower portion of the image, while NGC 3608 is in the upper portion.

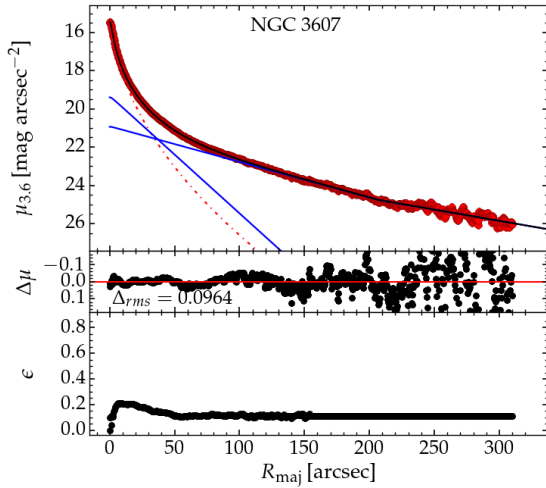


Figure A9. Alternative (questionable and not preferred) fit for NGC 3607 obtained by adding a large-scale anti-truncated disc (bent blue line: $\mu_0 = 20.91 \text{ mag arcsec}^{-2}$, $h_{\text{inner,maj}} = 58''.4 = 7.0 \text{ kpc}$, $R_{\text{bend,maj}} = 207''$, $h_{\text{inner,maj}} = 92''.4 = 11.1 \text{ kpc}$), plus two intermediate-scale discs, the smaller of which is fit with a Sérsic function (red, inner-most dot-dashed curve: $n_{\text{maj}} = 2.0$, $R_{e,\text{maj}} = 10''.3 = 1.24 \text{ kpc}$, and $\mu_e = 18.28 \text{ mag arcsec}^{-2}$) matching the strongly rotating component in the kinematic map (Krajnović et al. 2011) and the second with an exponential disc (straight blue line: $\mu_0 = 19.32 \text{ mag arcsec}^{-2}$, $h = 17''.7 = 2.1 \text{ kpc}$) matching the ellipticity profile.

A2 A couple of ellicular galaxies (ES)

A2.1 NGC 3607

The ES galaxy NGC 3607 is a merger product (Ricketts et al. 2009b) with a dust-rich inner disc. The kinematics presented by Krajnović et al. (2011) reveal that the fast-rotating inner disc, which extends to $R_{\text{maj}} \approx 15''$, is embedded within a larger, slower-rotating component. The behaviour of this inner embedded disc in the kinematic map is similar to that seen in NGC 3377, NGC 4473, and other ES galaxies (Arnold et al. 2014).

Fig. A8 provides a basic decomposition into two components, with a large-scale spheroid plus an inner component for this ES galaxy's embedded disc(s). The galaxy's total apparent magnitude is 9.27 mag. Conceivably, the upturn in the outer light profile ($\gtrsim 200''$) may be due to contamination from two neighbouring galaxies. Nonetheless, performing a fit within $R_{\text{maj}} = 220''$ and

again extrapolating the optimal fitted model to infinity dims the galaxy magnitude by just 0.06 mag. Using the initial brighter magnitude, along with a luminosity distance of 25 Mpc and an M/L ratio of 0.75, yields $\log(M_{\star,\text{gal}}) = 11.37 \text{ dex}$, which is 0.09 dex smaller than the value given in Graham & Sahu (2023a).

The elevation in the ellipticity profile extends to 45'' (Savorgnan & Graham 2016), suggesting an additional larger (than 15'') component is present. Some 17 per cent of the flux is assigned to the inner component (Fig. A8) associated with the spikes in the rotation profile (within $R_{\text{maj}} \sim 15''$) and the ellipticity profile (within $R_{\text{maj}} \sim 45''$). These two features are drawn out more clearly in Fig. A9, where the galaxy has been fit with a questionable large-scale anti-truncated disc. This fit yields the same total galaxy magnitude as obtained with the fit shown in Fig. A8 but is not preferred because a large-scale disc does not match the kinematic or ellipticity profiles at large ($\gtrsim 45''$) radii. The kinematic and ellipticity data sets NGC 3607 apart from NGC 3091. The fit shown in Fig. A9 has been included to help visualise how a heated thick outer 'disc' can produce a dynamically-hot spheroid-dominated (Fig. A8). The decomposition in Fig. A9 only applies *if* NGC 3607 has an overlooked face-on large-scale disc. Richings et al. (2011) report a depleted core with a break radius $R_b = 0''.22$ in NGC 3607.

A2.2 NGC 4291

Jedrzejewski & Schechter (1989) report $V/\sigma = 76/273 = 0.28$ for NGC 4291, which makes it a 'fast (inner) rotator', although the rotation falls from 100 km s⁻¹ at 3'' to 40 km s⁻¹ at 12'', before peaking again at $\sim 15''$ and then falling back down to $\sim 50 \text{ km s}^{-1}$ by 20'' (see also Bender et al. 1994). Therefore, there appear to be two components causing this rotation. This pattern is reflected in the ellipticity profile, which rises rapidly to peak at $\sim 15''$ before slowly declining. Indeed, Pinkney et al. (2003) speculated that NGC 4291 may be an ES galaxy.

The surface brightness profile is well represented by a dominant spheroid plus two inner components (Fig. A10). The total 3.6 μm magnitude is 10.96 mag, and the spheroid magnitude is 11.06 mag. At a luminosity distance of $25.2 \pm 3.7 \text{ Mpc}$, and with $B - V = 0.927$ and $M_{\star}/L_{3.6} = 0.78$, one has $\log(M_{\star,\text{sph}}) = 10.68 \text{ dex}$, which is 0.12 dex smaller than the total galaxy stellar mass reported by (Graham & Sahu 2023a) that was based on a single-Sérsic fit. This reduction is due in part (0.04 dex) to some re-assigned mass into the two extra components and in part (0.08 dex) because the revised spheroid Sérsic index declined (from 4.2 to 3.6 on the major axis), and thus the large-radius tail of the Sérsic pro-

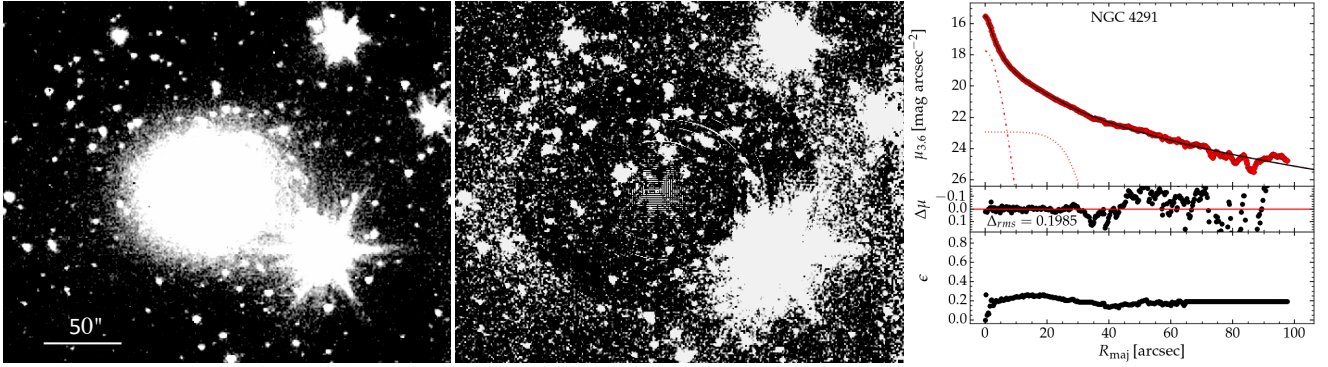


Figure A10. NGC 4291 retires its E galaxy designation to become an ES galaxy — image courtesy of *SHA*. The scale bar is $50'' = 6.05$ kpc long. The spheroid-to-total ratio is 0.91. Two inner components fit with Sérsic functions are detected, with the ellipticity profile suggesting a somewhat face-on disc in accord with the rotation reported in the literature. The dominant spheroid has $n_{\text{maj}} = 3.65$, $R_{e,\text{maj}} = 15''.2 = 1.84$ kpc, and $\mu_e = 20.03$ mag arcsec $^{-2}$.

file falls away more quickly, i.e., there is a little less extrapolated light at large radii.

The light profile for NGC 4291 appears to be a particularly good example of how an anti-truncated disc can morph into a single spheroidal structure well described by the Sérsic function.²³ There remains a hint of a double disc structure in the light profile. The next galaxy that is remodelled is NGC 5077. Although it has a similar light profile to NGC 4291, little to no trace of a double disc structure is apparent in its light profile. Nonetheless, the light profiles are still better modelled by including an inner and faint intermediate-scale component.

A3 A couple of elliptical galaxies (E)

A3.1 NGC 5077

NGC 5077 was thought to possibly display somewhat fast (inner) and slow (outer) rotation as far back as Bertola et al. (1991). While there is no clear stellar rotation within the inner $\sim 10''$, from ~ 10 – $28''$ there is systematic (ring?) rotation along the major axis, albeit at just 30 – 40 km s $^{-1}$ (Raimundo 2021). As such, this is not on par with the previous ES galaxies. Looking at the gas, rather than the stellar kinematics, NGC 5077 has a high-rotation (~ 300 km s $^{-1}$) polar gas disc that has been accreted (Bertola et al. 1991; Raimundo 2021). The accreted system may contribute to the additional components detected during the analysis of the light profile. The accretion event may also have damaged/eroded the inner portion of a previous intermediate-scale stellar disc aligned with the major axis. Such accretion events can invoke star formation in (what becomes disturbed) E galaxies (Biswas & Wadadekar 2024).

NGC 5077 has a total $3.6 \mu\text{m}$ magnitude equal to 10.49 mag, a luminosity distance of 39.8 ± 7.4 Mpc (Theureau et al. 2007), a Galactic-extinction-corrected $(B - V)_{\text{Vega}}$ colour of 0.99 mag and an $M_*/L_{3.6} = 0.90$, giving $\log(M_{*,\text{gal}}/M_\odot) = 11.37$ dex, just 0.04 dex less than reported in Graham & Sahu (2023a). From the decomposition shown in Fig. A11, $B/T = 0.8$ and the spheroid stellar mass is 11.27 dex. Arguably, some of the accreted material should now be considered a part of the spheroid and a logarithmic mass between 11.27 and 11.37 dex used for the spheroid. A possible de-

pleted core, with a major axis break radius of $0''.2$, was identified by Trujillo et al. (2004).

A3.2 NGC 6251

The supergiant E radio galaxy NGC 6251 (Waggett et al. 1977) is remodelled in Fig. A12. This Seyfert 2 galaxy has a one-sided jet — reported at radio wavelengths by Waggett et al. (1977) and Perley et al. (1984) — that can be seen in the residual image (Fig. A12, middle panel). The dominant spheroid’s Sérsic index equals 4.0, and its apparent magnitude equals 11.29 mag. The galaxy’s total magnitude is $\mathfrak{M}_{3.6,\text{gal}} = 11.18$ mag. At a distance of 105 Mpc, and with $M/L = 0.73$, one has $\log(M_{*,\text{gal}}/M_\odot) = 11.84$ dex, in good agreement with the value of 11.87 ± 0.15 dex reported by Graham & Sahu (2023a). The spheroid mass is slightly smaller, at 11.80 dex. Consequently, NGC 6251 resides rightward of the main E galaxy distribution in the $M_{\text{bh}} - M_{*,\text{gal}}$ diagram (Fig. 3). This situation could arise if NGC 6251 experienced multiple mergers, more like a BCG than a regular E galaxy, with dry mergers driving it rightward of the steep quasi-quadratic $M_{\text{bh}} - M_{*,\text{gal}}$ relation for E galaxies built by, on average, one major dry merger.

In an exploration for a large-scale disc, or perhaps a captured/assimilated outer rotating component or a halo of stars, Fig. A13 presents a potential but questionable solution. This is akin to what was done with NGC 3607 in Fig. A9. The exponential disc scalelength is $36''$ (17 kpc) before anti-truncation at $R_{\text{maj}} = 114''$ increases the scalelength to $98''$ (47 kpc). The reduced spheroid in Fig. A13 has $\log(M_{*,\text{gal}}/M_\odot) = 11.50$ dex. If applicable, NGC 6251 would join NGC 3091, reclassified as an S0 with an unusually large galaxy stellar mass around $5 \times 10^{11} M_\odot$. Should extended kinematic information become available and reveal rotation in NGC 6251 at $R_{\text{maj}} \gtrsim 20$ – $30''$, it might help solidify the disc-to-spheroid transition process as a route to the ‘Sérsicification’ of E galaxies. However, the exponential structure in Fig. A13 is very extended, reminiscent of the halos/envelopes around cD and BCGs that were discovered to have a tendency for exponential light profiles (Seigar et al. 2007). Although, despite residing in the $M_{\text{bh}} - M_{*,\text{sph}}$ diagram next to the second brightest Fornax Cluster galaxy, NGC 1399, NGC 6251 is in a poor cluster (Werner et al. 2000; Chen et al. 2011) and is, therefore, not expected to be surrounded by a halo of stars stripped from other galaxy cluster members.

²³ With *Hubble Space Telescope* resolution, NGC 4291 has a depleted core with a break radius equal to $0''.3$ (Dullo & Graham 2014).

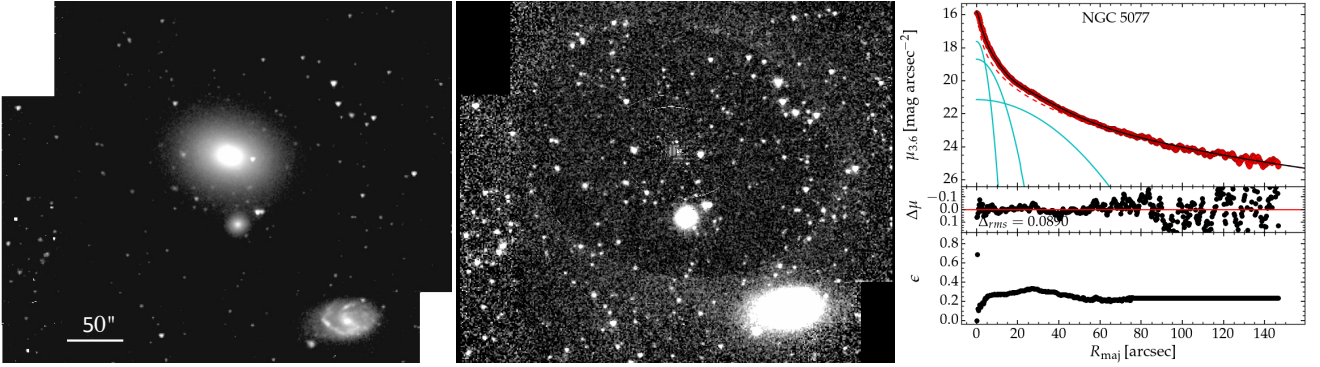


Figure A11. Similar to Fig. 1, but for NGC 5077, which retains its E galaxy designation, although it arguably may be considered an ES galaxy, like NGC 4291. Image courtesy of *SHA*. The scale bar is $50'' = 9.45$ kpc long. The light profile is decomposed into a Sérsic spheroid (dashed red curve: $n_{\text{maj}} = 4.40$, $R_{\text{e,maj}} = 39''.7$, and $\mu_{\text{e}} = 21.87$ mag arcsec $^{-2}$), a broad Gaussian ring aligned with the major axis and having a peak ring-to-spheroid flux occurring at $\sim 28''$ (Raimundo 2021), and two (near) nuclear components associated with unrelaxed accreted gas/dust aligned with the minor axis and is the reason why this is not considered an ES galaxy. The spheroid-to-total flux ratio is $0.80^{+0.05}_{-0.10}$.

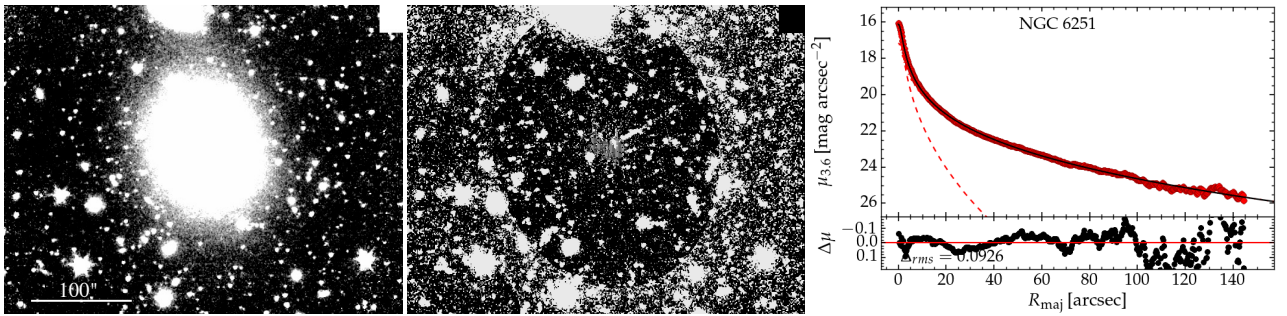


Figure A12. Similar to Fig. 1 but for the apparently ‘slow rotator’ NGC 6251, which retains its E galaxy designation. Image courtesy of *SHA*. The scale bar is $100'' = 48.3$ kpc long. A poorly constrained inner Sérsic function (dashed red curve: $n_{\text{maj}} = 1.5$, $R_{\text{e,maj}} = 3''.5$, and $\mu_{\text{e,maj}} = 19.57$ mag arcsec $^{-2}$) is included to accommodate the feature associated with the dust lane/disc(?); which contains 4 per cent (when $n = 0.5$) to 10 per cent (when $n = 2.5$) of the total flux, although this latter value is undoubtedly an upper limit due to the extrapolation of the Sérsic model. Arguably, NGC 6251 could be considered an ES galaxy. The dominant spheroid has $n_{\text{maj}} = 4.64$, $R_{\text{e,maj}} = 36''.5$, and $\mu_{\text{e,maj}} = 22.29$ mag arcsec $^{-2}$. The AGN jet is visible in the residual image.

A4 A brightest cluster galaxy (BCG)

A4.1 NGC 4486 (M87)

NGC 4486 is modelled in Fig. A14 with a core-Sérsic function (Graham et al. 2003), a small central point source, and an extended excess (perhaps an undigested meal) centred around $94''$ along the major axis. The galaxy’s magnitude is 7.96 mag. At a luminosity distance of 16.8 ± 0.8 Mpc (Event Horizon Telescope Collaboration et al. 2019), and using $M/L = 0.80$ (based on $B-V = 0.94$), one can derive $\log(M_{\star,\text{gal}}/M_{\odot}) = 11.58$ dex, 0.09 dex smaller than reported in Graham & Sahu (2023a).

This paper has been typeset from a $\text{\TeX}/\text{\LaTeX}$ file prepared by the author.

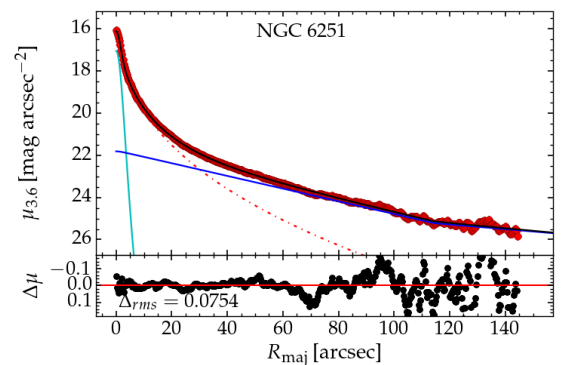


Figure A13. Alternative (questionable and not preferred) fit for the ‘slow rotator’ NGC 6251 obtained by adding an anti-truncated disc model (bent blue line: $\mu_0 = 21.78$ mag arcsec $^{-2}$, $h_{\text{inner,maj}} = 36''$, $R_{\text{bend,maj}} = 114''$, $h_{\text{outer,maj}} = 98''$) and using a Sérsic function with $n = 0.5$, i.e. a Gaussian (cyan curve: $\mu_0 = 15.53$ mag arcsec $^{-2}$, full-width-half-maximum = $1''.26$), for the inner component, yields a Sérsic bulge (red curve) with $\mathfrak{M}_{3.6,\text{sph}} = 12.02$ mag, $n_{\text{maj}} = 2.67$, and $R_{\text{e,maj}} = 10''.37$. The ‘disc’, or rather ‘halo’, magnitude in this fit is 11.76 mag, and the total magnitude is 11.09 mag.

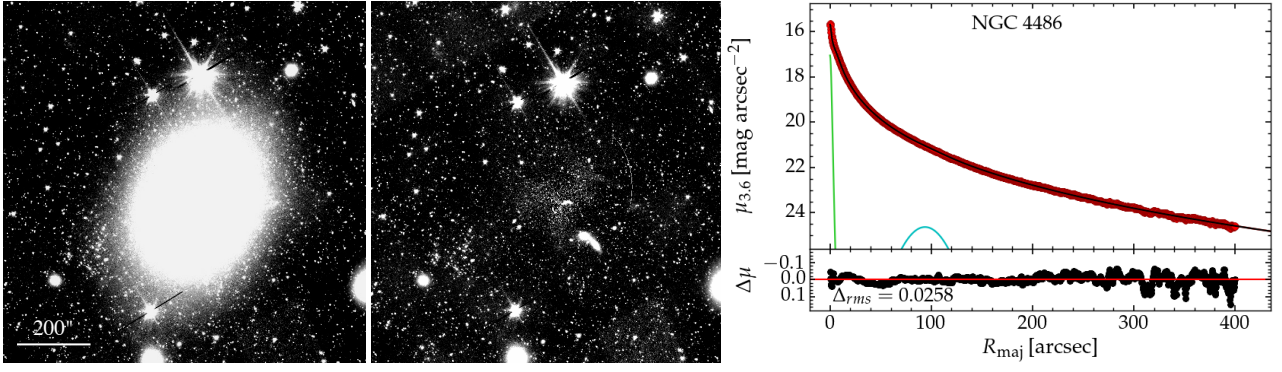


Figure A14. Similar to Fig. 1 but for NGC 4486, which retains its E galaxy designation. Image courtesy of S⁴G. The scale bar is 200'' = 16.2 kpc long. The light profile is decomposed into a central point-source ($\mathfrak{M}_{3,6,psf} = 15.04$ mag) plus a core-Sérsic spheroid ($n_{maj} = 4.83$, $R_{e,maj} = 100''.4$, $R_{b,maj} = 6''.7 = 0.54$ kpc, $\gamma_{maj} = 0.37$, and $\mathfrak{M}_{3,6,sph} = 7.99$ mag) and a Gaussian $\mathfrak{M}_{3,6,Gauss} = 12.22$ mag) to accommodate the extra light centred around 94''. The galaxy magnitude $\mathfrak{M}_{3,6,gal} = 7.96$ mag.